

We are IntechOpen, the world's leading publisher of Open Access books Built by scientists, for scientists

6,300

Open access books available

171,000

International authors and editors

190M

Downloads

Our authors are among the

154

Countries delivered to

TOP 1%

most cited scientists

12.2%

Contributors from top 500 universities



WEB OF SCIENCE™

Selection of our books indexed in the Book Citation Index
in Web of Science™ Core Collection (BKCI)

Interested in publishing with us?
Contact book.department@intechopen.com

Numbers displayed above are based on latest data collected.
For more information visit www.intechopen.com



Advanced Abrasive Waterjet for Multimode Machining

H.-T. (Peter) Liu, Vanessa Cutler,
Chidambaram Raghavan, Peter Miles,
Ernst Schubert and Nathan Webers

Additional information is available at the end of the chapter

<http://dx.doi.org/10.5772/intechopen.75313>

Abstract

Abrasive waterjet (AWJ) possesses inherent technological and manufacturing advantages unmatched by most machine tools. Recent advancements in AWJ processes have enhanced those merits. Multidisciplinary advancements include process automation, position accuracy, cutting models, range of part dimensions, ergonomics, user and environmental friendliness, feature recognition, and others. Among the technological merits, AWJ is material independent and a cold cutting tool, capable of preserving the structural and chemical integrity of parent materials. For heat sensitive materials, AWJ often cuts over 10 times faster than thermal cutting tools such as lasers and electrode discharge machining. Unlike photochemical etching, AWJ is environmentally friendly, producing no toxic byproducts. Additionally, AWJ requires only a single tool assisted with accessories to qualify for multimode machining; it is cost effective with fast turnaround for small and large lots alike. Recent advancements together with relevant R&D, engineering, and industrial applications will be presented for precision multimode machining from macro to micro scales.

Keywords: high pressure pump, micro abrasive waterjet, multimode machining, cold cutting, material independence, heat affected zone, cutting model, multi-passes

1. Introduction

Abrasive waterjet (AWJ) is a machine tool that removes materials by an erosion process of abrasive particles impacting the workpiece at supersonic speeds [1–3]. In [1], the history and fundamentals of waterjet technology and the early stage of the development of micro abrasive waterjet (μ AWJ) technology is described. This chapter is an update to report the

progresses in the evolution of μ AWJ and its impact on the overall advancement of waterjet technology.

AWJ inherently possesses several technological and manufacturing merits unmatched by most other tools [1]. The ones that are most relevant for precision machining are revisited below and expanded throughout this article.

- Material independence – cuts virtually any material, thin and thick
- Cold cutting – induces no heat affected zone (HAZ) and preserves structural and chemical integrity of parent materials
- Low force exerted on workpiece
- One tool qualified for multimode machining
- Broad range of part size from macro to micro scales
- No tooling requirement - cost effective with fast turnaround

In a 2005 marketing report, Frost and Sullivan stated that waterjet machine tools emerged as the fastest growing segment of the overall machine tool industry in the last decade, and this trend is expected to continue.¹ The lack of awareness among potential end-users, however, posed a stiff challenge to market participants on increasing the end-user base. Since then, waterjet technology has made advancements to take full advantage of its inherent merits. Waterjet performance has been elevated to the degree that it competes on an equal footing with conventional tools such as lasers, electronic discharge machining (EDM), and photo-chemical etching. In some cases, its performance greatly exceeds those of its conventional counterparts. The lack of awareness of these merits, though, still presents a considerable challenge to a broader acceptance as a precision machine tool.

2. Technical approach

The evolution of waterjet technology has focused on the development of software, hardware, and machining processes to take advantage of technological and manufacturing benefits. These developments focused on automating machining processes, improving machining precision and efficiency, minimizing environmental impact, enhancing ergonomics, ensuring user friendliness, and broadening capabilities toward multimode machining. At OMAX Corporation, this included software development of the Intelli-MAX® Software Suite to upgrade to new generations of cutting models and add new machining features aimed at precision and automated machining; hardware development and commercialization of micro abrasive waterjet (μ AWJ) for meso-micro machining and the development of novel processes concepts for machining various features.

¹Frost and Sullivan – “The World Waterjet Cutting Tools Markets” Date Published: 30 Aug 2005 (www.frost.com)

3. Equipment

3.1. JetMachining Centers

AWJ machining was carried out on several models of JetMachining Centers® (JMCs), including the MicroMAX® and the 60120®, as illustrated in **Figure 1**. The MicroMAX is one of the newest JMCs developed and commercialized under the support of an NSF SBIR Phase II grant for precision meso-micro machining. With the NSF SBIR Phase IIB supplemental funding, the MicroMAX was upgraded to incorporate a Tilt-A-Jet® (TAJ) for taper compensation and a Rotary Axis® for facing, turning, grooving, trimming, and machining other 3D features. The 60120 with a 3200 mm by 1575 mm cutting envelope was designed for machining large parts.

Three key accessories, the TAJ for taper compensation, the Rotary Axis for machining features on rotating workpieces, and the A-Jet 5-axis articulate head are options available for most JMCs, as illustrated in **Figure 2**. The combined operation of the Rotary Axis and the A-Jet is capable of machining many complex 3D features. A camera can be mounted next to the cutting head for precision locating and aligning features on workpieces.

3.2. Abrasive waterjet nozzles

Four AWJ nozzles were used: 14/30, 10/21, 7/15, and 5/10, each with orifice ID/mixing tube ID (in thousandth of inch). The diameter ratios are 0.36 mm/0.76 mm, 0.25 mm/0.53 mm, 0.18 mm/0.38 mm, and 0.13 mm/0.25 mm, respectively. The 7/15 is the smallest production nozzle whereas the 5/10 nozzle is a beta nozzle. A water-only nozzle is available for cutting relatively soft materials. **Figure 3** illustrates these nozzles. Garnet with sizes from 80 to 320 mesh was used as the abrasives in this investigation to machine parts with a wide range of part size and thickness.

3.3. Software

The software for automating waterjet cutting is the Intelli-MAX Software Suite. It includes a specialized CAD package LAYOUT, a user friendly controller MAKE, and an OMAX Interactive Reference (OIR) (<http://www.omax.com/waterjets/software>).



a.



b.

Figure 1. (a) MicroMAX and (b) 60120 JMC.

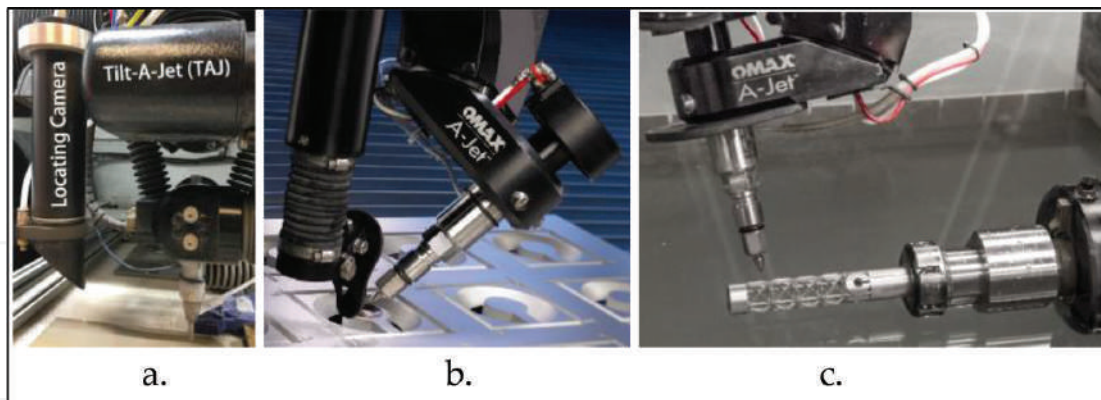


Figure 2. Accessories for 3D machining (a) TAJ (b) A-Jet (c) Rotary Axis.



Figure 3. Waterjet nozzles.

Intelligent software – The JMCs are controlled by a suite of software programs built around the patented motion control to automate the AWJ machining processes. Samples of the software suite are listed below.

3.3.1. Operational software

- **LAYOUT** is a full-featured CAD program created and designed to work with JMCs. Part drawings can be created by using a full set of drawing tools, importing a drawing from another CAD program in standard format such as DXF, or tracing a drawing or photograph. The toolpath of that part can then be created with LAYOUT.
- **MAKE** actually controls the JMC to create parts with several simple steps: (1) open a toolpath file created by LAYOUT (or another CAD/CAM drawing tool), (2) choose the material you want to use and its thickness (from which the exact nozzle motions required to make the part are calculated accurately, and (3) click on the “Begin Machining” to begin machining parts.

- **Intelli-MAX[®]** – a suite of new technologies integrated into the OMAX JMCs to enhance the performance of AWJ machining. It is designed to make higher tolerance parts faster – faster and with higher tolerance than any other AWJ systems. The suite has several software modules including Intelli-NEST for part nesting, Intelli-PIERCE for hole piercing, Intelli-TAPER to minimize edge taper, and Intelli-CORNER to corner compensation.

4. Results

One of the most recent advancements in waterjet technology was the development of micro abrasive waterjet (μ AWJ) technology for meso-micro machining. The merits of cold cutting, material independence, and low side force exertion on workpieces are keys to elevate the μ AWJ as a precision meso-micro machine tool.

For cutting heat-sensitive materials, waterjet is superior to thermally based machine tools such as lasers, electric discharge machining (EDM), plasma cutting, and others. The heat generated by these tools induces a heat-affected zone (HAZ) that alters the structural and chemical properties of the parent material. For thin materials, for example, the heat damage by CO₂ lasers results in considerable part warpage, formation of slag, or even vaporization of materials [2, 4]. The HAZ must be removed or minimized. Removal often requires grinding that is time consuming whereas minimization of the HAZ requires significant reduction in cutting power and therefore cutting speed.

Many machine tools are material limited. For example, lasers have difficulty cutting reflective materials such as copper; EDM cannot cut nonconductive materials; CNC hard tools meet with considerable challenges to cut hardened metals with large Rockwell indices. On the other hand, AWJ cuts most of these materials for a wide range of part size and thickness from macro to micro scales. In fact, AWJ cuts titanium 34% faster than stainless steel.

The low side force exertion on workpieces enables the AWJ to machine thin separations between features. Although the diameter of the μ AWJ nozzle is only capable of machining features such as the kerf width of slots and the diameter of holes in the meso scale range ($>200\ \mu\text{m}$), the separation or wall between these features is approaching the micro scale range ($<100\ \mu\text{m}$) [5]. Such a meso-micro machining capability is unmatched by most machine tools that do not offer the combination of cold cutting and low side force exertion.

By adding the MicroMAX into its product line, OMAX has established the full capability of multimode machining of most materials from macro to micro scales – the “7 M” advantage [3]. Considerable efforts have been devoted to conducting cutting tests and presenting the samples to demonstrate the versatility of waterjet technology as a whole. Selected tests and samples are presented herein.

4.1. High pressure pump

The only method we have to produce these very high pressures is through reciprocating motion. There is no turbine or other “continuous” mechanism that can do this. The two

types of electrical prime movers are the electric motor that rotates and a coil or solenoid that can directly produce reciprocating motion. The other prime mover is an internal combustion engine that starts out producing exactly the kind of reciprocating motion we require but in most cases this is converted to rotary motion through a crankshaft. This is then converted back to reciprocating motion in the pump. Waterjet pumps for industrial use are run by electric motors. Pumps for field use tend to be powered by internal combustion engines.

1. **Electric motor-intensifier:** These are the earliest systems, with the first commercially viable system having been developed by McCartney MFG originally for pumping catalyst in the polyethylene industry.² The electric motor drives a hydraulic pump. This hydraulic pressure is routed through a four-way valve system to either side of a hydraulic intensifier that results in reciprocating action and high pressure.
2. **Electric motor-direct drive pump:** This approach eliminates the hydraulic circuit. An electric motor drives a crankshaft that converts rotary motion to reciprocating motion. These systems can also be run by an internal combustion engine for field applications.
3. **Low speed electric servo motor – intensifier:** This uses a ball screw to convert low speed rotary motion to low speed reciprocating motion.

Hydraulic horsepower (HP): This is the HP delivered at the nozzle. All the power consumed by the electric motor ends up either as hydraulic HP that is the useful power, or as wasted power in the form of heat.

Efficiency: The electric power delivered to the motor is used up in the following ways:

- **Resistance heating**
 - Losses in the electric motor windings are proportional to the square of the current (i^2R). Motors can be designed with various efficiencies depending on windings. A normal efficiency of an electric motor is in the 90% range.
- **Conversion of rotary to linear motion**
 - The crankshaft is the most efficient method of doing this, as the forces are transmitted between two cylindrical surfaces with a lubrication film between them. The crankcase oil in a direct drive pump should not generally require any cooling system.
 - The hydraulic intensifier is the least efficient as it first converts the rotary motion of the motor to reciprocating motion of the hydraulic pump plungers which then pump a flow rate of hydraulic fluid 20–33 times the cutting water flow rate through a loop. This consists of passages in four-way valves and relief valves, causing pressure drops and heating. This fluid then has to move a large diameter piston that is connected to a smaller diameter plunger, and then return to the holding tank from where it is recirculated. The heat accumulates in the oil and has to be removed by pumping cold water through a heat

²“KMT McCartney Products for the LDPE Industry”. KMT McCartney Products. Retrieved 10 June 2012.

exchanger or a chiller. The cooling water flow rate may be 4–6 times the water used for cutting.

- In the low speed servo motor system, a servo motor drives a ball screw to convert rotary to linear motion. The ball screw is ideal for accurate position control of the XYZ axes but is highly inefficient at converting large amounts of power and huge forces from rotary to linear motion. These forces have to be conveyed across the small surface areas of the balls in the ball screw, creating a lubrication challenge. The lubrication system of the ball screw has to be separately cooled.
- **Friction** between the plungers and the guide bushings and dynamic seals create a small amount of heat in all pumps.
- **Check Valves** create heat when they leak and this is taken away by the cutting water that can also be used to cool the plungers and the dynamic seals.

Useful power/wasted power: This is the ratio of the two powers referred to above – the good vs. the bad. The lower the ratio, the worse the pump. The ratio for an intensifier can be one third that of an efficient direct drive pump.

Check valve design: A good seal requires high, even contact stress in the sealing zone. A ball on a cone does precisely this along a circle. A flat poppet on a flat seat is not the ideal way to seal a high pressure system. The probability of random debris getting between two flat surfaces is vastly higher than the probability of debris getting precisely on the ball-seat circle of contact. Second, if debris gets in between the flat surfaces it has no chance of escaping, whereas it gets pushed to one side or the other by the spherical surface of the ball and not cause damage. Third, the metal surfaces of the flat poppet and seat get eroded easily by high pressure water sneaking past on almost every stroke as the two surfaces cannot close in a manner precisely parallel to each other. These flat surfaces need frequent lapping, leading to more maintenance.

Constant and variable speed control: The bore of an orifice may vary by 2.5%. At a certain pressure, the difference in flow rate between these extreme sizes will be 5%. If a pump is set up to run at constant speed, producing a constant flow rate, the pressure drop across this range of orifice sizes will vary by 10%. In order to operate at a set pressure, a constant speed pump will have to be run at a higher speed to accommodate the larger size orifice and most of the time it will be dumping the extra water. Also, as the seals wear and the check valves erode, the output flow will drop and the pump will have to compensate for this and run constantly at an even higher speed. Constant speed pumps therefore run at about 10–13% higher speed than variable speed pumps and all this extra output is wasted. The variable frequency drive (VFD) adjusts the speed for the required pressure and avoids wastage.

When piercing holes, it is advantageous to drop the pressure to a piercing pressure. Doing this is easy with the VFD. An important application for waterjets is cutting composites and brittle piercing. Drilling starter holes in composites and in brittle materials requires the pump to shut off and start with the nozzle open. Direct Drive Pumps with a VFD can do this easily.

4.2. Micro AWJ technology

Under the support of an NSF SBIR Phase II grant, OMAX developed and commercialized μ AWJ technology, culminating the MicroMAX JetMachining Center for precision meso-micro machining.³ The MicroMAX was subsequently upgraded by incorporating the TAJ for taper compensation and the Rotary Axis for machining features on rotating workpieces. The MicroMAX was named a Finalist of the 2016 R&D 100 Award. The technological innovation and success in commercialization of the MicroMAX has led to OMAX's reception of the U.S. Small Business Administration (SBA) 2016 Tibbetts Award. NSF subsequently selected OMAX as a success story for its SBIR/STTR program (<https://www.sbir.gov/node/1308555>).

The MicroMAX takes advantage of most of the merits of waterjet technology. Success in making the MicroMAX available commercially has greatly broadened the waterjet machining applications. The meso-micro machining capability has led to penetrating several industrial sectors in which conventional waterjets are inadequate for R&D, prototyping, and production applications. These sectors include but are not limited to aerospace, biomedical, electronic/optic, engineering, and military applications.

For precision AWJ machining, consistent abrasive flow rate is essential. Garnet is mostly used for AWJ machining because of its low cost and superior performance as the abrasive. A rule of thumb to prevent nozzle clogging with abrasives is to use abrasives with mean particle size no larger than 1/3 of the bore diameter of the mixing tube. This is to avoid bridging of two large particles inside the bore. With the downsizing of AWJ nozzles, the particle size of the abrasive is proportionally reduced accordingly. It is well known that the finer the particle, the more difficult for it to flow under gravity feed. One of the common problems of feeding fine abrasive from a hopper is the formation of rat holes, resulting in unsteady mass flow [6]. As the rat holes are formed, flushing or flooding of fine abrasives would result when a positive pressure gradient builds up locally near the nozzle. Packing of fine abrasives also leads to positive pressure buildup. Under certain circumstances, a negative pressure gradient could build up just upstream of the nozzle. The presence of negative pressure gradient would reduce the flow rate of fine abrasives through the nozzle. In other words, fine abrasives flowing through the hopper would experience unsteady flow rate under the influence of buildups of positive and/or negative pressure gradients inside the hopper. The abrasive ceases to flow when the rat holes are fully developed. For the 5/10 nozzle, the finest abrasives can be used to assure consistent feeding is 240 mesh with a mean particle size of 60 μm . Since the surface roughness of AWJ-machined edges is proportional to the particle size, finer garnet such as 320 mesh with a mean particle size of 30 μm is often used to reduce surface roughness. Novel processes were developed to improve the flowability of fine abrasive 320 mesh and finer (US Patent 8920213 B2). **Figure 4a** and **b** shows three photographs of the flow patterns of unprocessed and processed garnet, respectively. When examining flow patterns of 320-mesh garnet exiting the feed gate of the hopper, the unsteadiness and inconsistency of the flow patterns of the unprocessed garnet is evident. Cutting with unprocessed fine garnet would lead to wavy kerf width and even skipped cutting [7].

Figure 5 shows a display board highlighting μ AWJ machined 2D and 3D parts cut from various materials such as metals (aluminum, steel, and titanium), nonmetal (glass, ceramics, carbon

³There are five US patents and one PCT patent application pending for μ AWJ technology

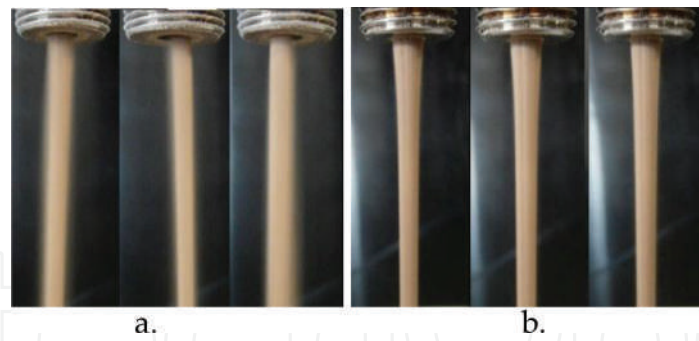


Figure 4. Flow patterns of unprocessed and processed 320-mesh garnet [7] (a) Unprocessed (b) Processed.



Figure 5. Photographs of μ AWJ-machined parts—An overview.

fiber, acrylic, polycarbonate, Garolite (G10), Poly-Ether-Ether-Ketone (PEEK), and honeycomb. Also, a simulated nanomaterial with large gradients of nonlinear material properties has been cut with AWJ [7]. These displays clearly demonstrate the merits of abrasive waterjet technology for material independence, no tooling requirements, and one single tool for multimode machining. There is simply no other machine tool capable of machining such a wide range of materials.

As a cold cutting tool that is materials independent, the μ AWJ was demonstrated to machine large-aspect-ratio slots on a 2.2 mm thick 440C stainless steel sheet that was heat treated to a Rockwell index of $R_c = 58$. The part is a bonding extender for lapping thin-film ceramic substrates. This μ AWJ machined part was cut on the MicroMAX using the 5/10 nozzle with 240-mesh garnet. **Figure 6** illustrates the μ AWJ machined part; **Figure 6a** and **b** correspond to the photographs of the entry and exit surface of the part. Pockets and patterns were precut on the blank before waterjet machining. The slots consisted of widths as narrow as 0.3 mm and lengths as long as 260 mm. In the absence of the HAZ, it took a single pass of the waterjet to machine the part in 23 minutes.

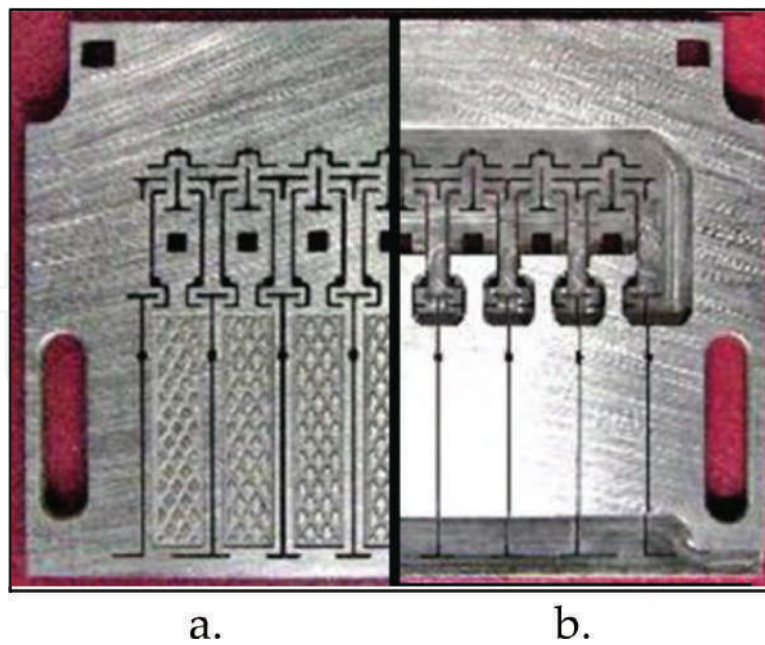


Figure 6. μ AWJ-machined complex slot patterns on hardened steel (Courtesy of Competitive Engineering) [2] (a) Entry side (b) Exit side.

For such narrow slots with large aspect ratios machined on highly hardened steel, it is extremely difficult if not impossible to cut using CNC hard tools as they often do not have the stiffness and tend to wear too rapidly to achieve the required tolerance. The current method to machine the part is by wire EDM. The EDM process requires three passes to cut each slot in order to minimize the HAZ. As a result, it took over 6 hours to cut the part. In other words, the cutting speed of the waterjet is better than 15 times faster than the wire EDM for comparable cutting quality.

With the TAJ activated, nearly taperless or square edges can be readily machined with waterjets. Several precision devices critically rely on square edges to achieve their optimum performance. Mechanical flexures are often used for accurate force measurements, precision motion control, and mitigation of backlash. In collaborating with MIT Mechanical Engineering, OMAX used the MicroMAX to machine prototypes of nonlinear load cells with large-aspect-ratio of thin flexures [8]. The patented design was capable of five orders of force range and its superior performance was verified through laboratory experiments [9, 10]. The close agreement between the theory and the experimental results was attributed to the nearly taperless edges of the large-aspect-ratio flexures.

As a part of Asteroid Redirection Mission (ARM) program, the Jet Propulsion Laboratory (JPL) of NASA has been developing prototypes of flexure-based microsplines to serve as the asteroid gripping device. The flexures consisting of several spring-like elements were originally machined with the wire EDM that must be cut with multiple passes at low speeds to minimize the heat damage in the presence of the HAZ such as surface hardening on the cut edges and distortion of the spring-like flexure elements. In collaborating with JPL, OMAX conducted a series of tests to machine several 3.2-mm-thick aluminum flexures. The single-pass cutting tests were conducted on the MicroMAX with the 7/15 nozzle together with 240-mesh

garnet. **Figure 7** illustrates several flexure elements that were supported only at two ends. With the TAJ activated, the cold cutting with extremely low side force exertion is essential for cutting such flexure elements with nearly taperless edges and very little distortion. The performance of the MicroMAX also met NASA's precision requirements. Based on the times required to machine these parts, the cost ratio of the waterjet and wire EDM was 1:14, leading to a cost saving of 93%. JPL has adopted the MicroMAX as one of the primary tool to continue the development and refinement of microsplines for the asteroid gripping device.

The Rotary Axis facilitates machining of features on rotating workpieces. Initially the LAYOUT drawing is the same as that of the 2D part. The features along the Y-axis are then converted to those in the rotary axis via the X-data, an algorithm that lets one input "extra" data for any entity in a drawing. After the tool path of the drawing is created, MAKE cuts the part by controlling the motion of the Rotary Axis to machine 3D features on the part. **Figure 8a** illustrates an interlocking link structure in a tube machined with AWJ. Machining the interlocking feature would be challenging for other machine tools. **Figure 8b** illustrates a titanium mesh cage, an implant used in spinal surgery to replace and reinforce the anterior column. A sacrificial rod was inserted into the tube while machining to protect the opposite wall from damaged by the spent AWJ. a titanium mesh cage, an implant used in spinal surgery to replace and reinforce the anterior column. A sacrificial rod was inserted into the tube while machining to protect the opposite wall from damaged by the spent AWJ.

4.3. Versatility of AWJ technology

With four product lines of waterjet systems equipped with accessories for 2D/3D machining and nozzles for wide range of part size and thickness, OMAX has established the full capability for multimode machining of most materials from macro to micro scales – the "7 M" advantage [3]. Several publications have been devoted to demonstrating the versatility of waterjet in terms of material independence and precision meso-micro machining capability [2–5, 7–10]. Inside the Engineering and the Demonstration Laboratories, cutting tests continue taking place to look for new applications on new materials. A part of the tests was conducted

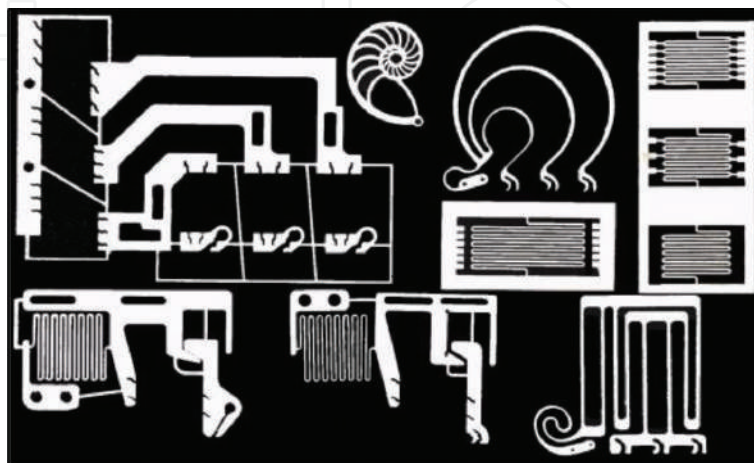


Figure 7. μ AWJ-machined aluminum flexures with flimsy spring-like elements (courtesy of NASA/JPL).

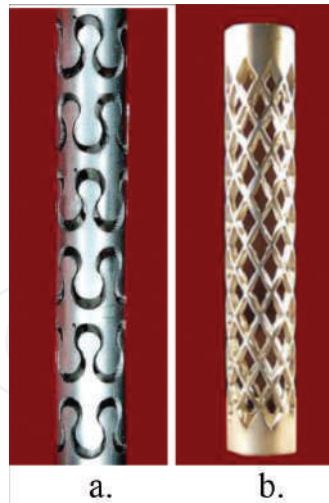


Figure 8. Two cylindrical parts machined with the rotary axis.

by the in-house R&D and Engineering Group. Many of them were requested from prospective clients before committing to purchase one or more of the machines. In this subsection, several applications to demonstrate the versatility of waterjet technology are described, in particular, those applications that are unique to waterjet technology.

4.3.1. 3D machining

The spent AWJ still consists considerable erosion power, if “not tamed,” could cause damage either to the operator or workpiece around the cutting nozzle. In other words, AWJs are not inherently suitable for 3D machining, particularly for parts with complex 3D features. Because the simplest and most effective means to dissipate the residual energy of spent abrasives is to let the spent AWJ shoot into a column of still water, most AWJ systems are built on top of a water tank that also serves to support the traversing mechanism. Such AWJ systems are generally designed for 2D machining. Novel methods and accessories were developed, within the constraints of operational safety, to machine 3D parts using 2D AWJ systems [11].

One of the simple methods to machine a 3D part on a 2D platform is to machine it multiple times in different orientations. As an example, **Figure 9** illustrates a model fighter plane machined on an aluminum rectangular block in three orientations.

Another example was to build a 3D assembly using many 2D components. **Figure 10** illustrates a model Boeing 777 aircraft (right half) that was assembled from AWJ-machined wing and nacelle cross sections, stabilizer, and rudders made from thin sheets of carbon fiber. Selected wing cross sections are shown in the upper left corner.

The Intelli-MAX Software Suite has incorporated several programs for machining parametric shapes, or pre-configured shapes that use equations to machine a shape without having to create the tool path first. One such program is the internal and external Gear, Rack and Sprocket Generator in both U.S. and metric standards. Using the 5/10 nozzle on the MicroMAX, several sets of miniature planetary gears made from titanium, PEEK (with and without fiber reinforce-

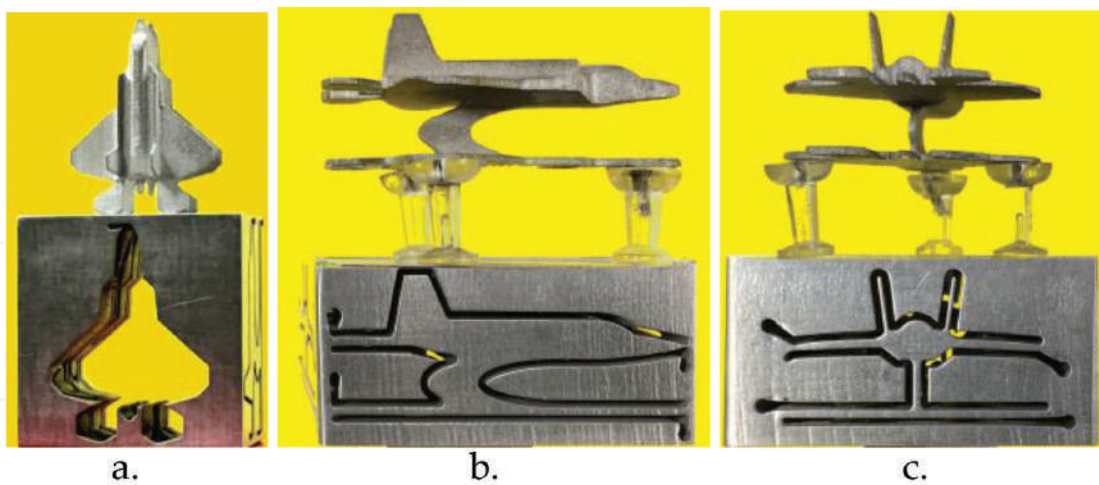


Figure 9. AWJ-cut 3D fighter aircraft—completed in three separate 2D cuts (a) Top view (b) Side view and (c) End view.

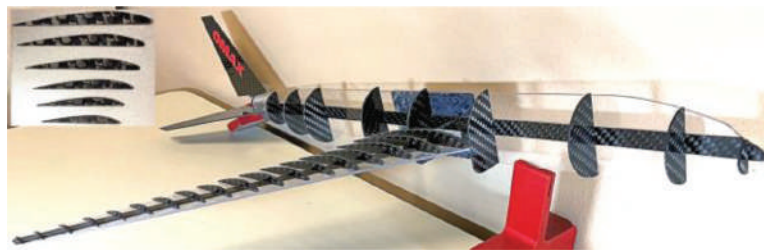


Figure 10. A Boeing 777 aircraft model assembled from AWJ-cut components made from carbon fiber [3].

ment) were machined and assembled into operating models [3]. One of the common gears is the cycloidal gear that is designed for watch making. **Figure 11** illustrates a set of miniature cycloidal gears cut with the 5/10 nozzle on the MicroMAX. The gears were made from titanium sheet 2.0 mm thick. They were assembled into two decks of gears driven by a micro motor (a 298:1 71 rpm micro spur gear head motor manufactured by Solarobotics, Model GM14a). The lower deck consists of a large gear (19.3 mm OD) and two small gears (5.4 mm OD). The upper deck consists of a large gear (12.7 mm OD) and three small gears (3.61 mm OD). The two decks of gears were separated by an acrylic plate. The two large gears were mounted on a common shaft that is driven by the micro motor powered by a 3 V button battery (Panasonic CR2477). The assembled AWJ as-cut gears run quite smoothly, demonstrating the adequacy of the precision of the MicroMAX. Our goal is to machine the components of a pocket watch and assemble the watch as a means to demonstrate the capability of the MicroMAX for precision micromachining.

As the first step to reach the above goal, we acquired online the DXF of a wood clock “Genesis” by Clayton Boyle [12]. The clock was designed for hobbyists with the components cut manually with a scroll saw or a router. High-quality plywood was recommended for making the main components such as the gears. This is an ideal case to demonstrate the gear and clock making capability of waterjet in terms of fast turnaround and precision. The DXF files of the Genesis components were imported to LAYOUT and compiled in MAKE.

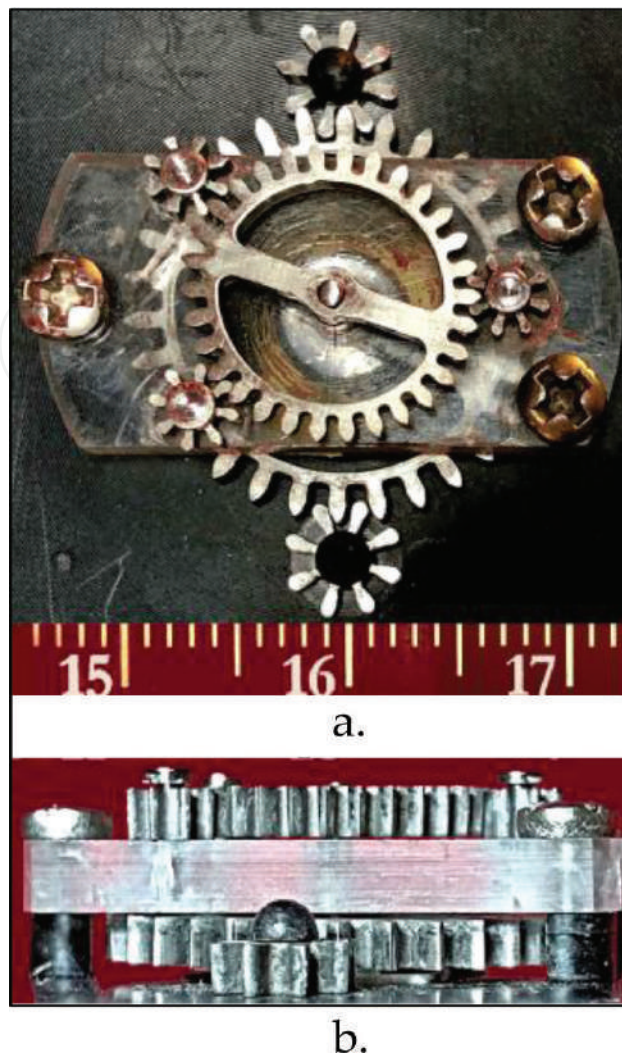
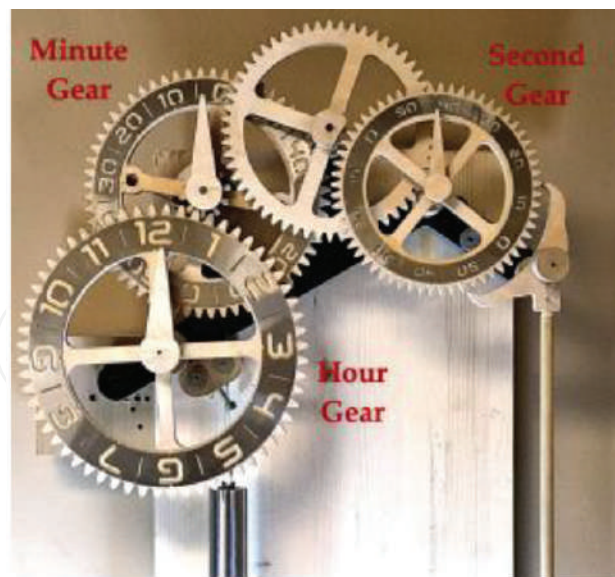


Figure 11. Cycloidal gear set (a) Top view (b) Side view.

All the components of the Genesis clock were then cut on a MAXIEM waterjet system in the OMAX Demo Lab in just hours as opposed to days using the scroll saw. **Figure 12** illustrates the assembled wood clock. The faces of the hour (lower left), minute (middle), and second (right) gears were cut from a thin stainless steel sheet. The clock is controlled by the adjustable length of the pendulum. The clock is driven by a 3.2 kg stainless steel bar that turns a click wheel attached to the back of the minute gear via a fish line. A small aluminum bar serves as the counter balance to straighten the fish line as the clock runs. Refer to Reference 12 for a detailed description of the clock.

For large bevels and countersinks, the A-Jet with a range of tilt angles from 0 to 60° to the vertical can be used. **Figure 13** illustrates a pair of beveled titanium honeycomb parts with 65 and 45° edge bevel angles, respectively; both the facesheet and the core were made of titanium. Note that cutting titanium honeycomb presents a considerable challenge to most machine tools. CNC hard tools tend to deform the thin core material whereas lasers and EDM must cut slowly to minimize the HAZ.



a.



b.

Figure 12. “Genesis” wood clock [12] (a) Top half (b) Lower half.

By combining the operations of the Rotary Axis and the A-Jet, complex 3D parts can be readily machined. One of the useful applications is to machine “fish mouth” weld joints for metal pipes, large and small, as illustrated in **Figure 14**. The joints are often cut with plasma cutting machines that leave a large HAZ on the cut edges. Removal of the HAZ often is done manually, leading to high labor costs and slow turnaround. The Intelli-MAX Software Suite has built-in programs to prepare tool paths for weld joints that can be cut with one of the JMCs. The as-cut joints are weld ready without the need of any secondary processing.

Another application is to machine inclined holes such as those used in aircraft engines [3]. For modern aircraft engines operating at very high temperature, there is a need for drilling inclined and shaped air breathing holes to achieve maximum cooling. The current practice requires a two-step process to drill inclined and shaped holes on TBC coated metal. First, the nonconductive TBC is removed with a laser and the hole in the substrate is drilled with an

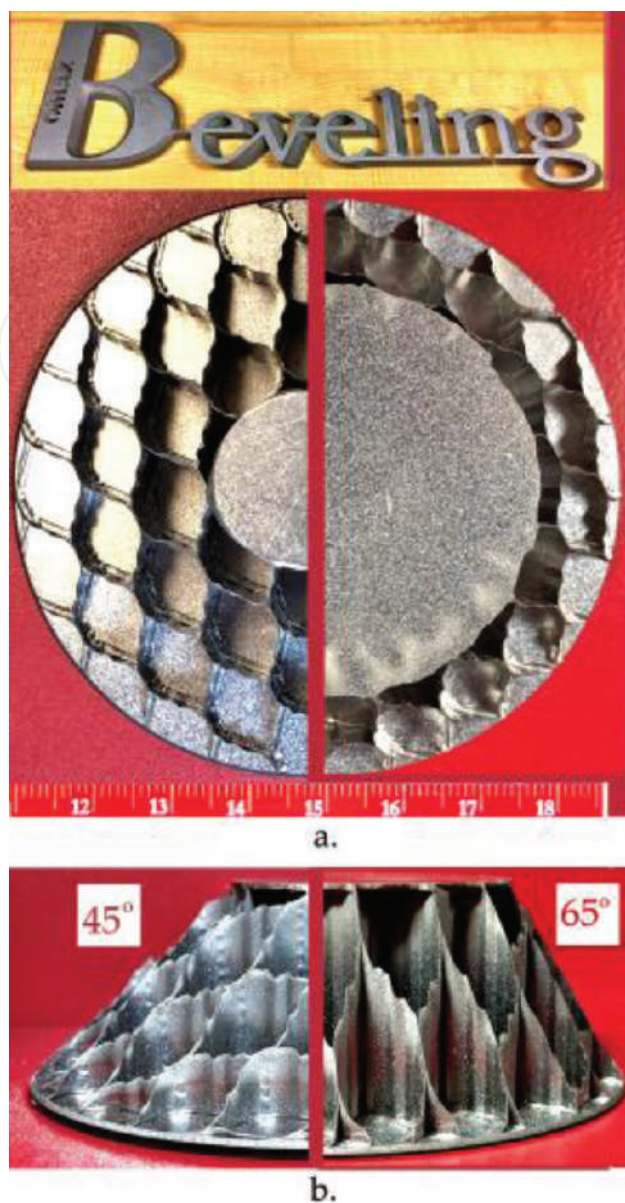


Figure 13. Beveled titanium honeycomb parts (a) Top view (b) Side view.

EDM process. The EDM process is very slow in order to minimize the HAZ damage. The AWJ was applied successfully to drill such holes on refractory metals with and without thermal barrier coating, as illustrated in **Figure 15**. In the absence of the HAZ, the AWJ drills holes much faster than CNC tools. By mounting the workpiece on the Rotary Axis, any inclined angle of holes can be drilled. The geometries of the holes were drilled by controlling the tilting of the A-Jet. Within certain limitations, the inclined angle and the shape can vary simultaneously along the hole axis. The AWJ nozzle consisted of a 0.18-mm ID diamond orifice and a 0.38-mm ID mixing tube. Garnet of 220 mesh with a flow rate of 45 gr/min was used. Seven hole geometries were drilled with a single nozzle on these samples to demonstrate the versatility of the AWJ in hole drilling. Most important, there was no delamination between the coatings and substrates and no HAZ on the hole edges on the substrates.



Figure 14. AWJ-cut “Fish mouth” weld joints.

4.3.2. Milling of glass mirrors

One of the more interesting applications for abrasive waterjets is controlled depth milling. Instead of cutting through the workpiece, the abrasive waterjet is traversed at a high speed across the part's surface. This causes the jet's kerf to change from a through cutting cross section to a grooving and then to an etching cross section. As the relative traverse rates increase between the nozzle and workpiece's surface, the penetration depth decreases. Precise depth control is achieved through a multi-pass process when, like with traditional milling operations, the final depth is achieved by walking the milled surface down to the final target depth. This is achieved by choosing a process where the amount of material removed per milling pass is less than the target depth tolerance. Depth control on the order of 0.03 mm can be achieved with the correct combination of process parameters.

When milling glass materials, the goal is to diffuse or reduce the power being applied to the surface of the part from a glass fracturing risk perspective. It is well known that cutting glass without abrasive results in fracturing the glass. Milling is no different, except that the fracturing tends to have more of a spalling damage. The key is choosing a set of process parameters where if the abrasive feed was interrupted, then glass will not break. This is achieved by using higher standoff distances on the order of 150–300 mm, orifice diameters less than 0.2 mm, mixing tube diameter to orifice diameter ratio's on the order of 10:1, and mixing tube lengths 100–300 mm, with jet pressures in the 70–200 MPa. The abrasive mass flow rate to waterjet mass flow rate ratio ranges from 25–100%. One of the keys is the traverse rates from 0.02 m/s to over 8 m/s. The higher the traverse rate, the more precise the depth control. The higher traverse rates are easier to achieve by spinning the work piece on a turntable.

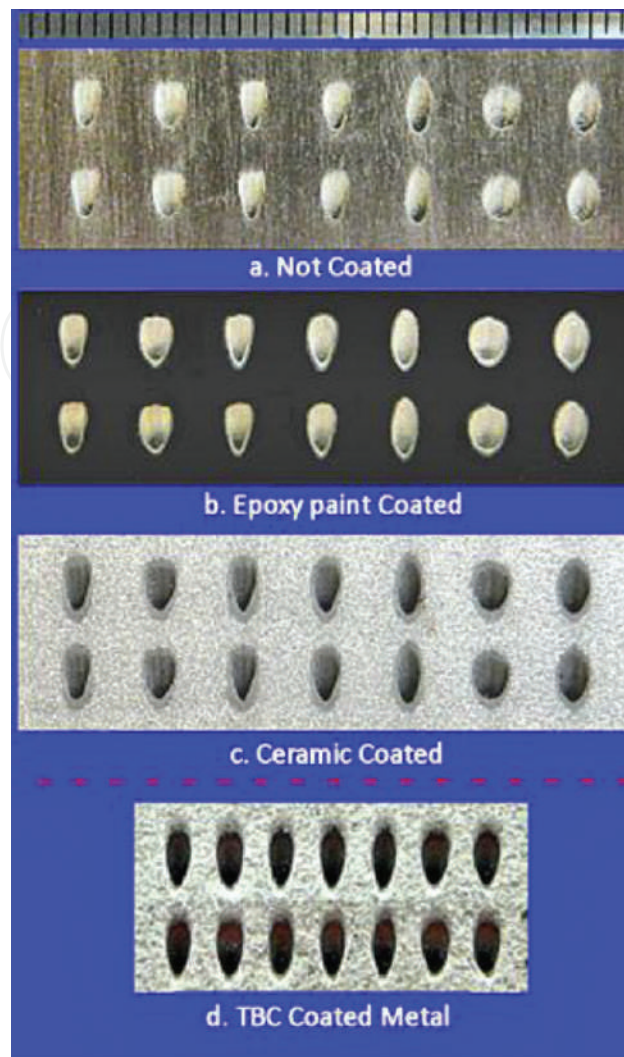


Figure 15. Inclined shaped holes on refractory metals.

One of the applications that the abrasive waterjet milling process has been successfully applied to is reducing weight in glass materials for ultralight-weight mirrors [13]. Samples include a 250 mm (major axis) elliptical mirror with pockets milled to a depth of 9.5 mm (**Figure 16**) and a 305 mm wide mirror made from 5.3 mm thick Ultra Low Expansion (ULE) glass with pockets milled to a depth of 3.6 mm (**Figure 17**). This mirror design was for testing of the active bending concept to change its focal point for phasing together multiple mirrors together for the James Webb telescope program.

These mirrors were milled with a milling process where the relative traverse rates were about 8 m/s. At these speeds, slowing the jet down to change directions without causing the jet to mill deeper as the jet speed decreased is mechanically impossible to accomplish. To solve this problem a mask with the lightweighting Isogrid pattern was placed on top of the glass, and the abrasive waterjet milling process is rastered across the entire surface of the mask. The mask was made from steel, and the relative erosion rate between the glass and steel is about 40 to 1. This allows for the mask to be reused on multiple parts before needing to be replaced.

Figure 18 shows an artistic milled pocket pattern that can be easily replicated dozens of times using the same milling mask.

Figure 19 illustrates how the jet rasters across the mask's surface. The glass is milled where all of the openings in the masks are located. Very intricate patterns can be milled into the glass surface. As a side note, one of the other advantages the abrasive waterjet machine has, is that the very same tool used to mill the glass can be used to cut the mask pattern. After each pass of the abrasive waterjet, the centerline of the jet is laterally indexed, as shown in **Figure 20**. When the index distance is approximately 70% of the mixing tube diameter, the milled surface produced is smooth and flat.



Figure 16. 250 mm (major axis) elliptical mirror with pockets milled to 9.5 mm deep.



Figure 17. 305 mm wide mirror made from 5.3 mm thick ultra-low expansion glass with pockets milled to 3.6 mm deep.

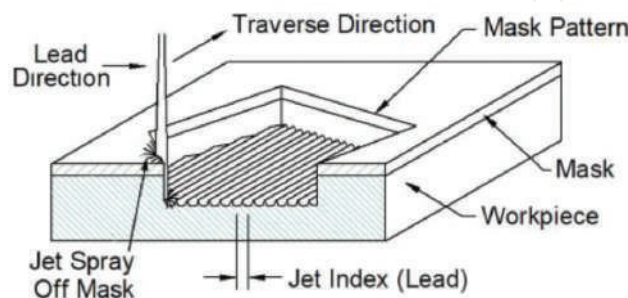


Figure 18. Masking the pattern.

4.3.3. Machining glass artworks

Glass that is often used as a comparison material for industrial comparative testing is a great material to demonstrate the versatility of AWJ. Known as a strong and brittle material, glass has a variety of applications across industries, including the creative sector. Exploration to generate artworks that investigate the waterjet process in the medium of glass was conducted. Working in a variety of scales the process remains the same with slight considerations regarding the delicacy, intricacy and complexity of the design [14]. **Figure 21** illustrates two artwork examples by assembling multiple layers of AWJ-machined pieces.

The design process can start in a variety of different ways, such as importing a vector file from any software capable of saving a drawing as a vector file (e.g., Rhino, AutoCAD, Illustrator and SolidWorks). The process of cutting is a two dimensional process and therefore requires a single outline. The initial programming is undertaken in various softwares and nested into the machine's software before cutting. The files are made and saved as a vector such as a DWG or DXF file. In work such as the "Scrutiny" handwriting was photographed and saved as a

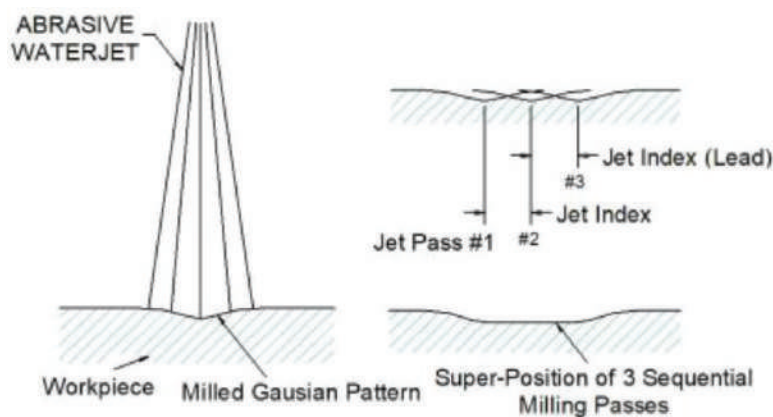


Figure 19. Superimposing successive milling passes to generate flat surfaces.

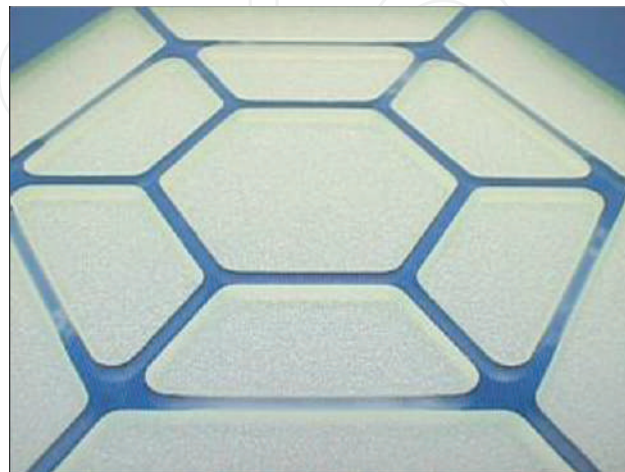


Figure 20. Artistic masked milling.

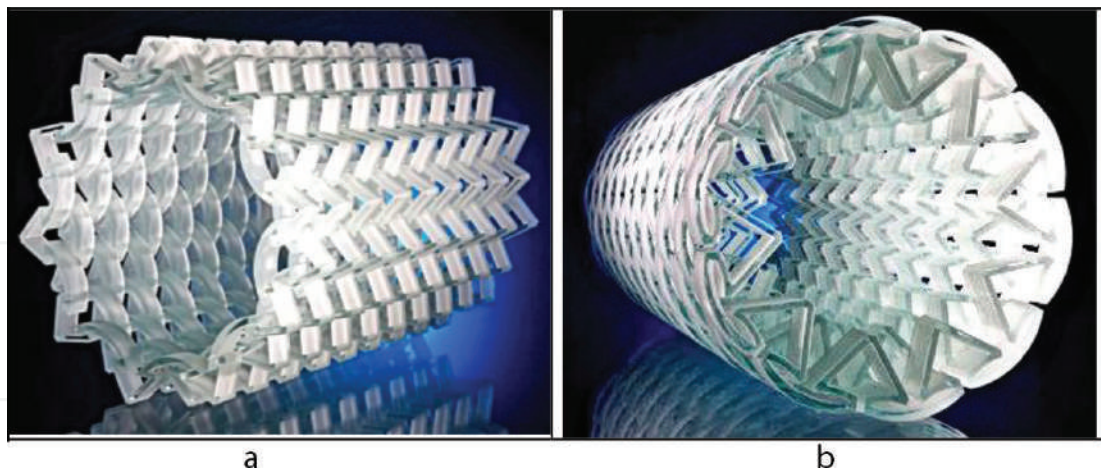


Figure 21. AWJ-machined artwork examples (a) Multi-layers of AWJ-cut glass (b) “Intertwine” glass sculpture.

JPEG and imported into the OMAX Intelli-TRACE software, where the writing was adapted within the software to fit within a given surface area [15].

The process is able to capture detail and work to tight tolerances and variable angles to effectively capture the handwriting. The AWJ can cut through stacks, working with glass thicknesses from 1 mm to over 65 mm using a variety of soda-lime, clear float glass and various artist glass stacks such as Bulleye.⁴

A variation in speed of abrasive flow, standoff distance, and how the machine is set up along with the order and direction of cutting can have effect on obtaining a successful outcome. Optimum pump pressures depending on the work undertaken varies between 11,000 and 58,000 psi. Higher pressure pumps have been used but with the application of multiple pierce points and variation of pressure from high to low, a lower pressure pump has proved more suitable due having to ramp from low to high pressure multiple times. Maintaining a consistency of pressure and abrasive is crucial in cutting glass. In cutting the handwriting, rhino board was used for the more delicate forms with water not covering the head in case a splash fractured the glass. Other handwriting at 2 mm thickness and not as complex, the work was cut underwater. **Figure 22a–c** illustrates the processes for machining handwriting on glass.⁵

For 5-axis cutting, the consideration with glass is how the material is held in place, as well as the order and priority of cutting. Most work is cut sitting on a surface tilted to reduce the residual wastes falling away. Another consideration is “taper lock,” which can trap the form within the waste material. There is a lot more risk with a brittle material such as glass; residual stress within the material can causing internal fracturing especially in thicker glass material. Cutting a form in glass can have different programming to that of a metal form and its set up is crucial to a successful outcome.

⁴A brand of fusing glass that allows various colored glass to be used together that have the same coefficient that make the glass compatible with each other.

⁵Photography credit: Simon Bruntnell

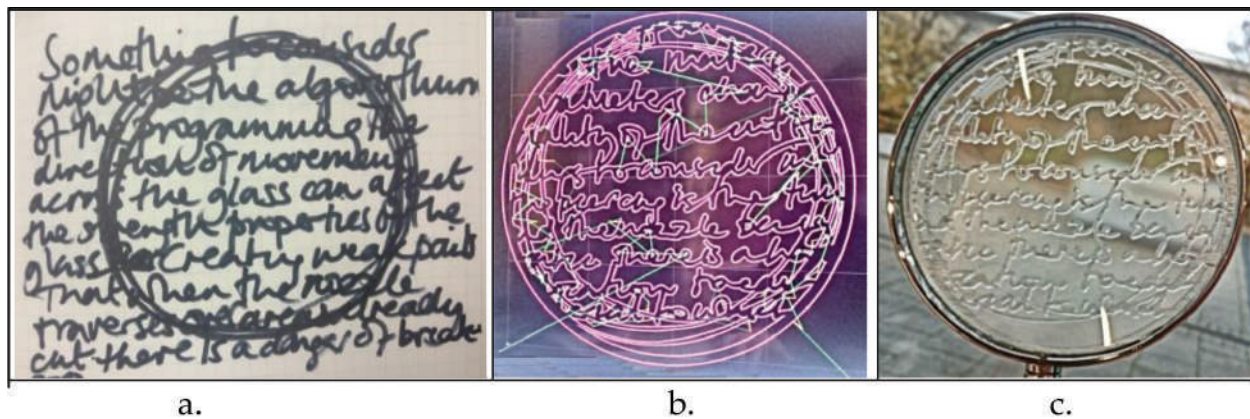


Figure 22. Processes for AWJ-machining of handwriting on glass [15] (a) Initial drawing sketch (b) Tool paths and (c) Micro glass handwriting.

4.3.4. Piercing of composites

Composites, laminates, and brittle materials have long been difficult materials to process by conventional machine tools such as mills and lathes as well as abrasive water jets and other beam cutting technologies. Most of the issues involved in shaping involve either peculiarities with the materials' heat sensitivity, brittleness, low tensile strength or its abrasive nature. Rapid wearing of alloy drills has been one of the main concerns that degraded the precision and repeatability of machined features. Early tests revealed similar damage took place during the initial hole piercing process with AWJ. Considerable efforts were subsequently made in an attempt to understand and mitigate such damage [3, 16–17]. It was discovered that damage occurred whenever the buildup of stagnating pressure inside blind holes exceeds the tensile/adhesive strength of composites/laminates' binder. Based on the above understanding, novel processes to minimize the stagnating pressure were developed for piercing composites/laminates without inducing damage. The Turbo (patented) and Mini Piercers were developed for AWJ drilling of large and small holes, respectively. **Figure 23** illustrates AWJ-machined internal features that require piercing on composite (G10), laminate (aluminum), brittle materials (glass and silicon wafer) with no damage.

Another advantage of using AWJ to machine composites is that the nozzle, unlike drill bits, does not come in direct contact with the workpiece. In other words, the nozzle wear is independent of the property of composite workpiece. For certain composites that are highly abrasive, excessive and rapid wear was experienced by the drill bits. Such rapid wearing of the drill bits and cutting tools tends to degrade the precision and repeatability of the machined features [18]. On the other hand, the AWJ nozzle wears considerably slower than the drill bits do. For extremely precise parts, AWJ can be readily used as a near-net shaping tool. The part can then be finished by light trimming with a precision hard tool. As such, the tool life can be greatly extended.

4.3.5. Patient-specific orthopedics and prosthetics

At present, most orthopedic and prosthetic implants are mass produced with limited sizes to achieve an average fit for individual patients. Since the implants are not tailored to the specific patient, it is not possible to optimize the implant operation for an optimum match. Recently,

there has been strong advocacy for manufacturing patient specific implants for optimum fitting, with a slogan of "one patient, one implant." Waterjet technology with its technological and manufacturing merits is most suitable for manufacturing such implants cost effectively with fast turnaround.

Waterjets are expected to lower the manufacturing cost of implants because of its no tooling requirement. As a cold cutting tool, all parts can be machined including secondary processes,

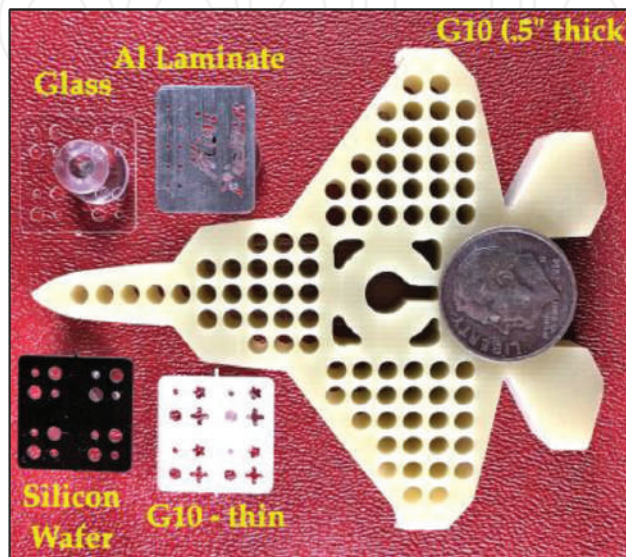


Figure 23. Piercing with Turbo and mini piercers.

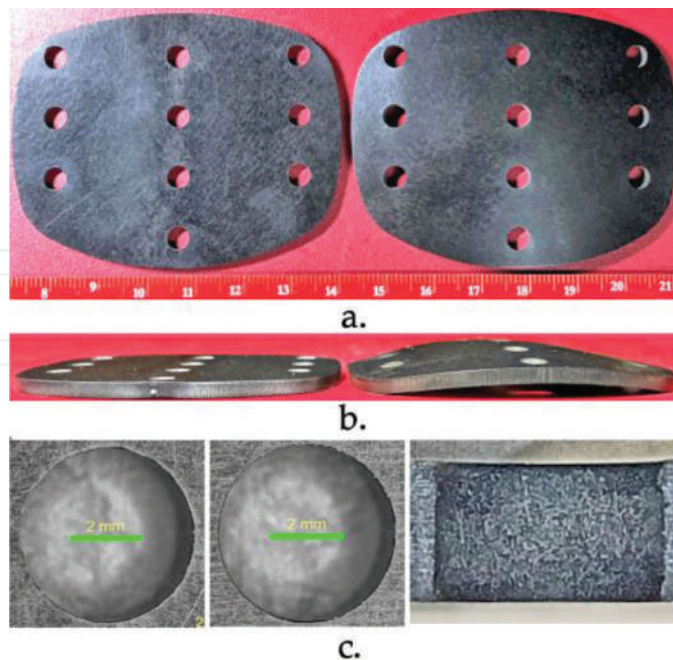


Figure 24. AWJ-machined cranial implants made from PEEK with fiber reinforcement (a) Top view (b) Side view and (c) Top, bottom, and side view.

if needed, in a matter of minutes or hours, depending on the complexity of the parts. Such fast turnaround is a must for in-situ implant operations. Furthermore, a mobile waterjet system has been applied successfully in remote areas such as the battlefield for rapid response repair [19]. The ruggedness of the system would facilitate setting up waterjet systems in remote areas for machining implants to broaden the reach of quality healthcare to underprivileged populations.

The applications of AWJ machining of biomedical components made of biocompatible metals such as titanium and stainless steel have been given elsewhere [11, 20]. An example of an AWJ-machined titanium mesh cage is illustrated in **Figure 8**. A relatively new biocompatible material, Polyether-Ether-Ketone (PEEK), has been shown to be a superior replacement of titanium implants in terms of avoidance of allergic tissue reaction to metallic ion and transparency to X-rays [21]. Success in applying waterjet for machining PEEK implants would greatly reduce the manufacturing costs together with fast turnaround. **Figure 24** illustrates AWJ-machined internal features that require piercing on the PEEK material with carbon fiber reinforcement. On the right of **Figure 24a** and **b**, the curved implant was thermally shaped at 316°C. **Figure 24c** shows the micrographs of the top, bottom and side views of one of the holes. Note that the hole edges were cut cleanly with no fiber hanging out loosely.

5. Conclusion

With the commercialization of micro abrasive waterjet or μ AWJ technology, the full capability has established for precision multimode machining of most materials from macro to micro scales for a wide range of part size and thickness. This “7 M” advantage of waterjet technology, together with cost effectiveness and fast turnaround, has greatly broadened manufacturing applications from R&D, prototyping, to 24–7 production of both small and large lots. The technological and manufacturing merits of waterjet technology have elevated it as one of most versatile machine tools unmatched by others. Specifically, the material independence and low side force exertion on workpieces are two most outstanding technological merits. A collection of AWJ-machined samples, made from a wide range of materials from metal, nonmetal, and anything in between, were presented to demonstrate the versatility of waterjet technology for a broad range of applications. In particular, machining many such examples presents considerable challenge to other machine tools in terms of material property, part geometry, tool performance, equipment/production costs, and machining/turnaround time.

It is concluded that recent advancement has elevated waterjet as a mainstream machine tool, often competing with lasers, EDM, and others on equal footings. For certain applications, waterjet outperforms its competitors. For cutting heat sensitive materials with low tolerance in heat damage, waterjet is at least 10 times faster than lasers and EDM.

Acknowledgements

This work was supported by an OMAX IR&D fund and NSF SBIR Phase I and II Grants #1058278. Any opinions, findings, and conclusions or recommendations expressed in this

material are those of the authors and do not necessarily reflect the NSF's views. The authors wish to thank the technicians in the Demonstration Laboratory for assistance in machining some of the parts illustrated in this article.

Author details

H.-T. (Peter) Liu^{1*}, Vanessa Cutler², Chidambaram Raghavan¹, Peter Miles¹, Ernst Schubert¹ and Nathan Webers¹

*Address all correspondence to: peter.liu@omax.com

1 OMAX Corporation, Kent, Washington, United States

2 Independent Waterjet Specialist and Glass Artist, Hampshire, United Kingdom

References

- [1] Liu H-T, Schubert E. Micro abrasive-waterjet technology. In: Kahrizi M, editor. *Micromachining Techniques for Fabrication of Micro and Nano Structures*. INTECH Open Access Publisher; 2012. pp. 205-234. DOI: 10.5772/1364
- [2] Liu PH-T. Mint: Precision machining of advanced materials with abrasive waterjets. IOP Conf. Series: Materials Science and Engineering, 164, 2017. 012008 DOI:10.1088/1757-899X/164/1/012008 (5th Global Conference on materials Science and Engineering, 8-11 November 2016, Tunghai University, Taiwan)
- [3] Liu H-T. "7M" advantage of abrasive waterjet for machining advanced materials. *Mint: Journal of Manufacturing and Materials Processing*. 2017; 1(11): 1-19 MDPI, Basel, Switzerland. DOI: 10.3390/jmmp1010011. <http://www.mdpi.com/2504-4494/1/1/11/pdf>
- [4] (Peter) Liu H-T. (2015) Abrasive-waterjet machining of most materials from macro to micro scales, In: *Proceedings 2015 TechConnect World Innovation Conference and Expo*; 14-17 June 2015; Washington DC. pp. 39-42
- [5] Liu H-T. Versatility of micro abrasive waterjet technology for machining nanomaterials. *Dekker Encyclopedia of Nanoscience and Nanotechnology*, 3rd ed. 2017. pp. 1-18. DOI: 10.1081/E-ENN3-120054064
- [6] Watanoa S, Imada Y, Hamadab K, Wakamatsub Y, Tanabeb Y, Davec RN, Pfefferc R. Mint: Microgranulation of fine powders by a novel rotating fluidized bed granulator. *Mint: Powder Technology*. 2003;131:250-255
- [7] Liu PH-T. Roles of abrasives in AWJ meso-micro machining. In: *Proceedings of 22nd International Conference on Water Jetting*; 3-5 September 2014; the Netherland. pp. 151-165

- [8] Liu PH-T. Roles of taper compensation in AWJ precision machining. In: Proceedings of the. 23rd International Conference on Water Jetting; 16-18 November 2016. Washington: Seattle. pp. 33-46
- [9] Kluger JM, Slocum AH, Sapsis TP. Beam-based Nonlinear US Patent No. 9599180 B2; 2016
- [10] Kluger JM, Sapsis TP, Slocum AH. High-resolution and large force-range load cell by means of nonlinear cantilever beams. *Precision Engineering*, 43, 2016. 241-256 (<http://dx.doi.org/10.1016/j.precisioneng.2015.08.003>)
- [11] Liu H-T, Olsen JH. Application of AWJ for 3D machining. In: Proceedings of the 2013 WJTA-ICMA Conference and Expo; 9-11 September 2013; Houston, Texas
- [12] Boyle C. Genesis [Internet] 2018. Available from: <http://lisaboyer.com/Claytonsite/Genesispage1.htm> [Accessed: January 07, 2018]
- [13] Miles P. Lightweighting large optics with abrasive Waterjets. In: Proceedings of SPIE, Novel Optical Systems and Large Aperture Imaging, 3430; 1998
- [14] Cutler V. *New Technologies in Glass*. London: Bloomsbury; 2012. 128 p. ISBN 978-1-4081395-4-7
- [15] Webers N, Cutler V. Interpreting handwritten scrawl. In: Proceedings of 23rd International Conference on Water Jetting; 16-18 November 2016; Seattle, Washington. pp. 99-109
- [16] Liu H-T, Schubert E. Piercing in delicate materials with abrasive-waterjets. *Mint: The International Journal of Advanced Manufacturing Technology*. 2009;**42**(3-4):263-279. DOI: 10.1007/s00170-008-1583-5
- [17] Liu H-T, Schubert E, McNeil D, Soo, K. Applications of abrasive-waterjets for precision machining of composites. In: Proceedings of SAMPE 2010 Conference and Exhibition, 17-20 May 2010; Seattle, Washington; 2010
- [18] Khashaba UA. Drilling of polymer matrix composites: A review. *Mint: Journal of Composite Materials*. 2013;**47**(15):1817-1832. DOI: 10.1177/0021998312451609
- [19] Anderson M, editor. Watercutting in Wartime [Internet]. 2013. Available from: <http://sme.org/MEMagazine/Article.aspx> [Accessed: Decemeber 29, 2017]
- [20] Liu H-T. Abrasive-waterjet technology for biomedical applications, In: Proceedings 21st Internal Conference on Water Jetting; 19-21 September 2012; Ottawa, Canada. pp. 99-112
- [21] Kurt SM, Devine JN. PEEK biomaterials in trauma, orthopedic, and spinal implants. *Mint: Biomaterials*. 2007;**28**(32):4845-4869

We are IntechOpen, the world's leading publisher of Open Access books Built by scientists, for scientists

6,300

Open access books available

171,000

International authors and editors

190M

Downloads

Our authors are among the

154

Countries delivered to

TOP 1%

most cited scientists

12.2%

Contributors from top 500 universities



WEB OF SCIENCE™

Selection of our books indexed in the Book Citation Index
in Web of Science™ Core Collection (BKCI)

Interested in publishing with us?
Contact book.department@intechopen.com

Numbers displayed above are based on latest data collected.
For more information visit www.intechopen.com



Grinding Force of Cylindrical and Creep-Feed Grinding Modeling

Pavel Kovač and Marin Gostimirović

Additional information is available at the end of the chapter

<http://dx.doi.org/10.5772/intechopen.76968>

Abstract

This chapter presents an experimental study of grinding forces as relationship of work-piece speed v , feed rate s_a and depth of cut a . For the modeling of cylindrical grinding used was response surface methodology and genetic algorithms. Modeled was the tangential force F_t and the normal force F_n in cylindrical grinding. The process included measurement of cutting forces during cylindrical grinding and later calculating their values using abovementioned techniques and determined adequate models. This chapter also examines the value and character of cutting forces in the creep-feed grinding. In order to identify the impact of cutting forces on the state of the process of creep-feed grinding, according to the elements of the machining experimental tests, relationship of the tangential and normal components of the grinding force and ratio of grinding force were determined. In comparison with the traditional multi-pass grinding results, the occurrence of higher cutting forces in creep-feed grinding, especially normal components, is shown.

Keywords: cutting force, cylindrical grinding, modeling, genetic algorithms, creep-feed grinding

1. Introduction

Knowledge about machinability of materials parameters, tool wear, quality of machined surface, cutting temperature, cutting forces, and so on, is beneficial not only for cutting process but also for designing the machine tools, fixtures, tools and process management. This was the goal of many researches especially in cutting, but there are only few data regarding grinding [1].

Research in grinding is performed with the purpose to define machining parameters, roughness of machined surface, grinding forces and grinding temperatures [2, 3]. Forces in surface grinding are measured with dynamometer Kistler, and they are increasing with increase of the material removal rate. Cutting forces measurements, during cylindrical grinding, are realized with dynamometer Kistler and are shown in [4].

Mathematical models of grinding force and grinding temperature for three wheels were established in [3]. Then, the role of chip formation force and friction force in grinding was investigated, and the thermal distribution in contact zone between workpiece and wheel was analyzed based on the mathematical model.

Grinding process is generally used to improve the tolerance integrity and surface integrity of a workpiece. It is crucial to know process forces since they are necessary to identify the conditions for surface burn. In [5], a new semi-analytical force model for grinding process was developed by modeling abrasive grits and their interaction with the workpiece material. Semi-analytical equations for normal and tangential force components as well as average force per grit are established by using the micro milling analogy. The model can then be used in prediction of the forces for different cases involving the same material and the abrasive grain however with different conditions.

In [6], a new grinding force model was developed by incorporating the effects of variable coefficient of friction and ploughing force. This is based on the fact that chip formation during grinding consists of three stages: ploughing, cutting and rubbing. Equations for the total normal and tangential force components per unit width of the grinding during these three stages were established. These components were expressed in terms of the experimental coefficients and process parameters like wheel speed, table feed and depth of cut. All the coefficients were determined experimentally by performing grinding tests at specified conditions according to the experimental trifactorial central composition plan.

Investigation of grinding force and grinding temperature of ultra-high-strength steel Aermet 100 in conventional surface grinding using a single alumina wheel, a white alumina wheel and a cubic boron nitride wheel was done in [7]. First, mathematical models of grinding force and grinding temperature for three wheels were determined. Then, the role of chip formation force and friction force in grinding force was investigated and thermal distribution in contact zone between workpiece and grinding wheel was analyzed based on the mathematical model. The experimental result indicated that the ratio of minimum grinding force to the maximum grinding force under the same grinding parameters can be achieved when using a CBN wheel and a single alumina wheel, respectively.

Proper understanding of the grinding forces can be useful in designing grinding machine tools and fixtures. Additionally, information on specific energy helps in selecting process parameters for achieving optimum output [8]. In this chapter, analysis of the effects of process parameters, tribology, work material and auxiliary equipment on grinding forces and specific energy, has been carried out. Existing models have been critically analyzed, and Werner's specific force model was found to be quite promising for advanced grinding processes. It was found that under specific boundary conditions and environment similar to advanced grinding processes, this model estimates grinding forces with acceptable accuracy [9].

Optimal control of workpiece thermal state in creep-feed grinding using inverse heat conduction analysis was done in [10] and surface layer properties of the workpiece material in high-performance grinding were analyzed in [11]. An inverse heat transfer problem for optimization of the thermal process in machining was done in [12].

For determination of dependence between cutting forces and machining parameters, firstly the full factorial experiment second-order design is used by [13]. With this approach, it is possible to determine the dependence of machining parameters and the results with minimal number of experiments.

This chapter analyzes the cutting forces in the creep-feed grinding and experimentally determined mean values of cutting force of abrasive grains that are currently in the grip with the workpiece as well. Cutting forces are determined depending on the treatment regime for two types of corresponding wheels.

As a second option for modeling, the dependence functions are genetic algorithms. They are extensively described in [14], and the same principle is implemented in this chapter.

1.1. Genetic algorithms

Genetic algorithms (GA) mimic the process of natural evolution by incorporating the “survival of the fittest” philosophy. In GA, a point in search space (binary or decimal numbers) is known as chromosome. A set of chromosomes is called population. A population is operated by three fundamental operations as follows:

1. reproduction (to replace the population with large number of good strings having high-fitness values)
2. crossover (for producing new chromosomes by combining the various pairs of chromosomes in the population).
3. mutation (for slight random modification of chromosomes).

At the very beginning, an initial population of 50 individuals is created. They are randomly generated from interval 0–1 using uniform distribution for creation of population. This indicates that real number coding was used. As a fitness scaling function, rank method was used. Most fit individual with the best raw score is assigned as first on the scaling list. Next to fittest is ranked number 2 and so on. This method is ranking every individual in generation as compared to the best individual in that same generation, no matter how good or bad fitness value is. And It was selected because it allowed the fastest convergence toward the best solution.

Selection of individuals for presence in mating pool was executed by roulette wheel method. Size of area on wheel occupied by a single individual is defined by rank score—the better the score, the bigger the area. Wheel is then spun and individual with the largest area has the most chances to be assigned a slot in mating pool. This action is repeated until all slots in mating pool are assigned. In each generation, two of the best individuals are automatically transferred to next generation. This act is called elitism and it guarantees that best genetic material is passed onto next generation. By setting this parameter high, the genetic diversity

is quickly reduced which leads to prolonged convergence time. On the other hand, setting it low, elite genetic material of every generation may be lost and algorithm stuck in local minimum. Number of individuals created by heuristic crossover is, in this case, 43. Heuristic crossover is carried out by creating children that randomly lie on the line containing the two parents, a small distance away from the parent with the better fitness value and in the direction away from the parent with the worse fitness value. After transferring two elite individuals from previous generation and creating 43 by crossover to complete a full population with 50 members last 5 individuals are created by mutating 5 of their predecessors.

With the process of mutation, a completely new genetic material is introduced into the population which helps in expanding genetic diversity and search space. It also prevents jamming an algorithm in a local minimum of the function. Uniform mutation is selected with the rate of 0.2. This type of mutation is basically a two-step process. In the first step, the algorithm selects a gene of an individual for mutation where each gene has the same probability as the mutation rate of being mutated. In the second step, the algorithm replaces each selected entry by a random number selected uniformly from the range for that entry. This whole process of selection, recombination and mutation lasted 500 generations.

2. Experimental investigation

2.1. Mathematical model

The abovementioned methodology of trifactorial central composition plan design was used during investigation in cylindrical grinding. Input parameters during modeling were machining parameters:

- Workpiece speed v (m/min)
- Feed rate s_a (mm/rev)
- Depth of cut a (mm)

Output parameters were:

- Tangential force F_t (N)
- Normal force F_n (N)

Other parameters were kept constant: tool geometry, tool wear, cooling and lubricating fluid, dynamical system machine-tool-workpiece.

Chosen mathematical model for grinding forces has the form:

$$F_i = C \cdot v_r^x \cdot s_a^y \cdot a^z. \quad (1)$$

2.1.1. Creep-feed grinding

In the case of surface grinding, where there is no lateral movement of the table, usually resulting force has been divided into tangential (extensive) component F_t and normal (radial) component F_n [6, 15].

Tangential component acts in the direction of the tangent to the surface of the grinding wheel and workpiece contact, that is, in the direction of cutting speeds. The normal component acts normally to the surface of the wheels and workpiece. As the diameter of the wheel is far greater than the depth of cut, it can be assumed that the tangential and normal component supine in a horizontal or vertical plane, **Figure 1**.

The relationship of normal and tangential components of the grinding forces is defined as the grinding force ratio:

$$\lambda = \frac{F_n}{F_t} = \frac{F'_n}{F'_t} \quad (2)$$

In the previous equation, the components of the grinding forces are reduced per unit width of grinding b , referred to as the specific grinding force:

$$\begin{aligned} F'_t &= \frac{F_t}{b} \\ F'_n &= \frac{F_n}{b} \end{aligned} \quad (3)$$

Grinding force can be expressed by specific grinding energy, which shows how much energy is consumed per unit volume of material removed:

$$u = \frac{P'}{Q'} = \frac{F'_t \cdot v_s}{a \cdot v_w} = \frac{F'_t}{h_m} \quad (4)$$

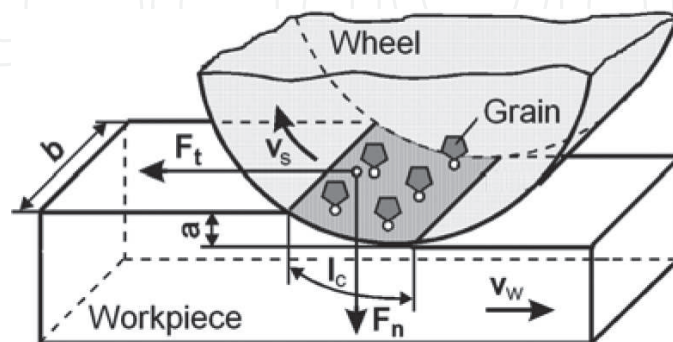


Figure 1. Components of the cutting force during creep-feed grinding.

2.2. Conditions during the experiment

2.2.1. Cylindrical grinding

Workpieces were cylindrical shaped $\varnothing 60 \times 150$ mm and were made from two types of steel:

- Steel EN 34Cr4. with mechanical properties $R_{p0.2} = 460$ MPa; $R_m = (690-840)$ MPa
- Steel EN 18CrNi8. with mechanical properties $R_{p0.2} = 485$ MPa; $R_m = (1080-1330)$ MPa

Tool was cylindrical grinding wheel $\varnothing 350 \times 40 \times 127$ mm, type B60L6V. Machining was performed on cylindrical grinder by manufacturer LŽTK Kikinda type UB, with dimensions of the workplace 1000×400 mm and power was rated 4 kW. Cutting speed was kept constant at $v_s = 3.65$ m/s. Varied machining regime parameter values: work speed v_r , feed rate s_a and depth of cut a are shown in **Table 1**.

2.2.2. Creep-feed grinding

Workpiece material used in the experimental setup was the molybdenum high-speed steel (HSS), which is widely used in the industry of cutting tools. Designation of the selected speed steel is DIN S 2-10-1-8. This steel belongs to a group of ledeburite steel with a microstructure consisting of martensite and fine mixtures of primary and secondary ledeburite cementite. The chemical composition of the test material was: 1.08% C; 0.22% Si; 0.23% Mn; 0.014% P; 0.019% S; 4.1% Cr; 1.5% W; 9% Mo; 1.1% V and 8% Co. Measured hardness on all samples ranged 66 ± 1 HRC. Experimental samples consisted of tiles measuring $40 \times 20 \times 16$ mm.

Based on the recommendations, the chosen material of the workpiece and set the conditions of processing were selected two wheels similar characteristics: wheels "Norton" type 32A54 FV BEP and size $400 \times 80 \times 127$ mm, respectively "Winterthur" type 53A80 F15 V PMF and size $400 \times 50 \times 127$ mm. The wheels are with high-quality abrasive grain, medium grain size, hardness soft, open structure with ceramic binder. All experiments were conducted with sharp wheels, and sharpening is done with a diamond planer alignment with a depth of 0.01 mm/speed and displacement of 0.1 mm/rev.

The machining conditions included variable depths of cut and workpiece speed. The depth of cut was $a = 0.05; 0.1; 0.25; 0.5; 1$ mm and the workpiece speed was $v_w = 2.5; 5; 10; 25; 50$ mm/s. The adopted mean value of specific material removal rate is $Q' = 2.5$ mm³/mm·s. The grinding wheel speed was constant $v_s = 30$ m/s.

2.3. Measurement of grinding force components

2.3.1. Cylindrical grinding

Resulting grinding force can be divided into three components (**Figure 2**):

- Tangential component F_t (acts in vertical direction)
- Normal component F_n (acts horizontally)
- Axial force F_a (acts in the direction of workpiece axis-feed)

No.	Machining factor			Experimentally measured values				Calculated values by response surface methodology			
				EN 18CrNi8		EN 34Cr4		EN 18CrNi8		EN 34Cr4	
	v_t [m/min]	s_a [mm/rev]	a [mm]	F_t [N]	F_n [N]	F_t [N]	F_n [N]	F_t [N]	F_n [N]	F_t [N]	F_n [N]
1	18.4	20	0.01	11.8	17	10.9	17.8	12.31	20.36	11.87	20.48
2	36.8	20	0.01	12.4	17.8	11.8	19.8	12.67	21.43	12.39	21.71
3	18.4	30	0.01	12.3	18.4	13	18.9	12.56	21.40	12.42	20.97
4	36.8	30	0.01	12.9	19.8	13.2	21.1	12.92	22.53	12.97	22.23
5	18.4	20	0.02	16.1	29	17.4	29	15.37	28.23	15.64	27.51
6	36.8	20	0.02	16.6	31.5	17.9	31.2	15.81	29.71	16.33	29.16
7	18.4	30	0.02	17.2	31.2	18.8	33.1	15.68	29.66	16.36	28.16
8	36.8	30	0.02	17.5	33.3	20	33.6	16.13	31.22	17.09	29.86
9	26	25	0.014	12.1	25.4	12.3	24.8	14.06	25.16	14.22	24.65
10	26	25	0.014	12	25.3	13.5	24.7	14.06	25.16	14.22	24.65
11	26	25	0.014	12.6	24.5	12.2	24	14.06	25.16	14.22	24.65
12	26	25	0.014	12.8	24.3	14	24.1	14.06	25.16	14.22	24.65
13	16	25	0.014	13.6	23.1	12.6	22.8	13.79	24.27	13.79	23.66
14	42.4	25	0.014	14.2	25.6	13.6	25.6	14.35	26.08	14.66	25.69
15	26	18.4	0.014	14.4	22.1	12.4	23.1	13.85	24.23	13.74	24.21
16	26	32.6	0.014	15.5	28.2	14.1	24.3	14.25	25.99	14.64	25.03
17	26	25	0.0086	11	19.2	10.8	19	12.03	20.00	11.71	20.03
18	26	25	0.023	17.1	33.2	18.1	31.1	16.48	31.78	17.32	30.45
19	16	25	0.014	13.4	23	12.1	22.5	13.79	24.27	13.79	23.66
20	42.4	25	0.014	14.5	25.8	13.9	25.7	14.35	26.08	14.66	25.69
21	26	18.4	0.014	14.2	22.9	12.6	23.3	13.85	24.23	13.74	24.21
22	26	32.6	0.014	15	28.1	14.6	24.1	14.25	25.99	14.64	25.03
23	26	25	0.0086	11.1	19.2	11	19.6	12.03	20.00	11.71	20.03
24	26	25	0.023	17.6	33.3	18.5	31.8	16.48	31.78	17.32	30.45

Table 1. Measured and calculated values of cutting forces.

During cylindrical grinding, axial force component F_a can be neglected because it is minor in comparison with F_t , which allows a much simpler dynamometer design.

Until now, two-component dynamometer with strain gauges was used for cylindrical grinding force monitoring. The same will be used in this experiment. Strain gauges were placed on both centers which enable reliable and accurate measurement of both components of cutting force on whole length of the workpiece.

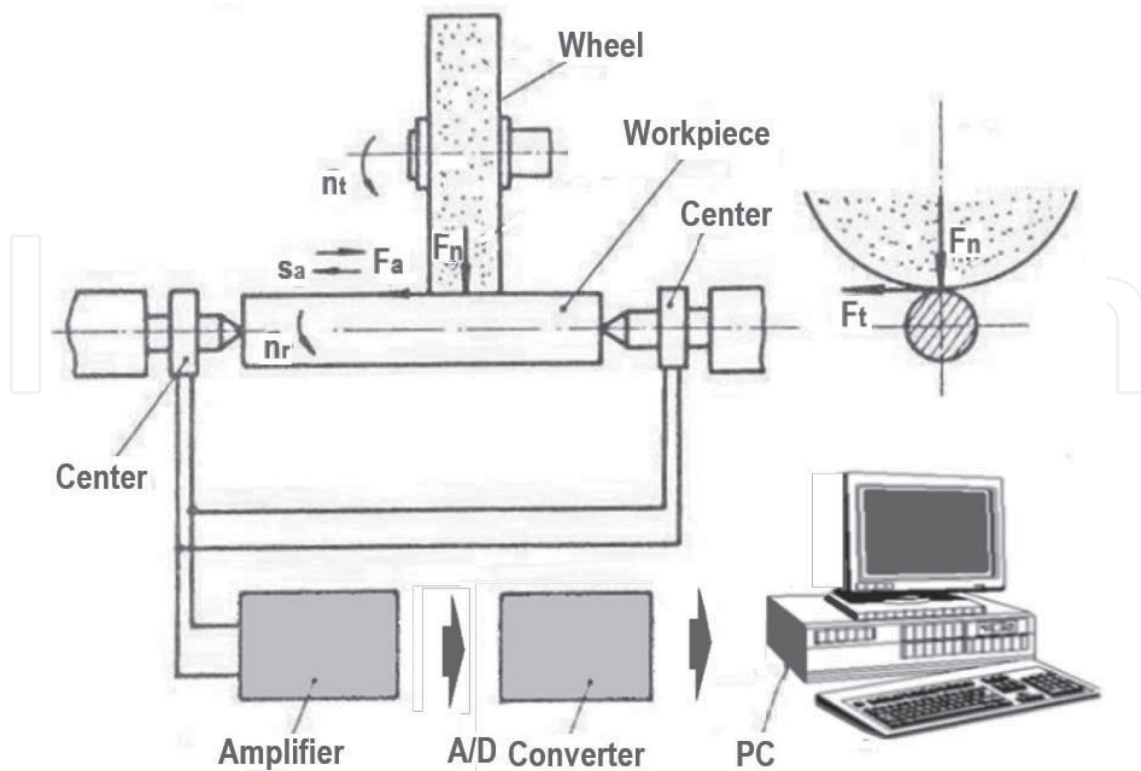


Figure 2. Information system for monitoring and processing cutting forces during cylindrical grinding.

Dynamometers were constructed in the manner that four strain gauges were taped onto cylindrical part of the center. In this way, two of the strain gauges are in the horizontal direction and two are in the vertical direction. All strain gauges are connected to bridge, so every component can be measured independently.

During grinding, under the influence of cutting forces, centers are deformed in the vertical and horizontal planes which are measured by strain gauges. Deformation of the strain gauge is proportional to load and signals coming from them have to be amplified and registered. To determine the cutting resistance values, dependence between measured signal (voltage on bridge) and load, $F_i = f(U)$, is determined with the use of lever and weight.

Mentioned measurement technique is accurate enough, but some things have to be considered:

- Quality of the glue used to stick strain gauges onto revolving centers
- Possible differences between electrical properties of strain gauges
- Accuracy of strain gauges positioning into vertical and horizontal planes
- Protecting the strain gauges from environmental influence
- Quality of the acquisition system
- Length of the cables to transfer measured signal

During the experiment, standard cemented carbide revolving centers are used.

Signals from dynamometers on centers were amplified with Kistler CA 5001 amplifier. Afterward, those signals were transformed by A/D converter to PC computer for further processing and analysis of measured data, **Figure 2**.

2.3.2. Creep-feed grinding

Measuring the forces that occur during creep-feed grinding was done using three-component dynamometers “Kistler Instrument AG,” type 9257. The used dynamometer works on the piezoelectric principle, which is reflected in the emergence of electricity on the surface of the crystal plate embedded in the dynamometer when the same force exerted pressure. Electricity is amplified by means of amplifiers capacitive “Kistler,” type CA 5001 and then is converted into DC voltage in the range from 0 to 10 V.

Measurement, analysis and control of the grinding force were performed using the information of the measuring system [10], where data acquisition is implemented by AD cards and cash integrated software package, **Figure 3**. The set information measurement data acquisition system is characterized by a high degree of accuracy, reliability, speed of response and the ability to reproduce measurement results. It allows real-time measurements, timely intervention if they appear illogical results, as well as comprehensive and rapid processing and analysis of results.

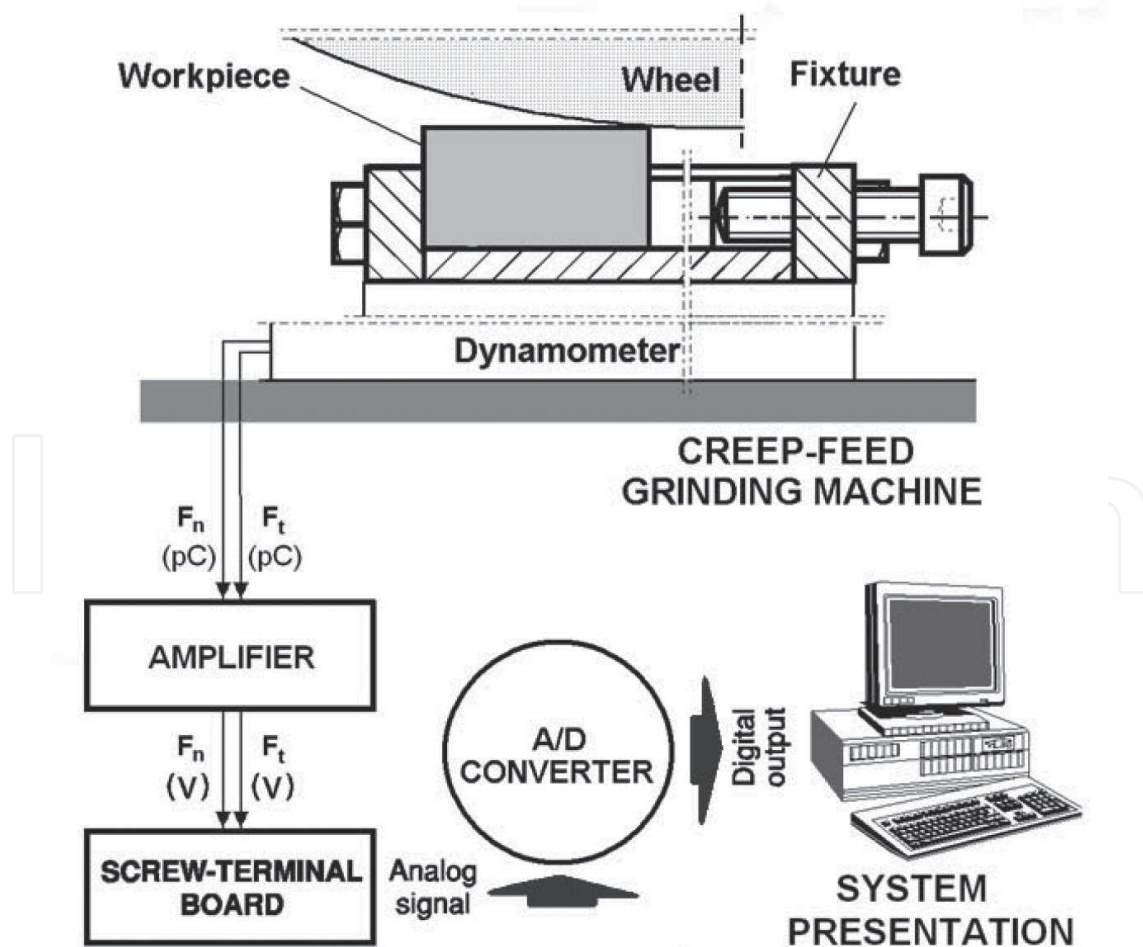


Figure 3. Information system for measuring and processing cutting forces during creep-feed grinding.

3. Analysis of experimental data

3.1. Cylindrical grinding

Based on the experimental plan and with the use of experimental devices, grinding forces values F_t and F_n are measured and recorded. Measured and calculated values for different machining parameters are shown in **Table 1**. On each sample of the material used for machining, for every experimental point, three repetitions were done, and the mean value of the repetitions was used in calculation of models.

Processing of the experimental data is performed with full factorial second-order design [9]. Side by side comparison of modeling with the genetic algorithms that were used to generate four coefficients from Eq. (1) while keeping the overall average error minimal is performed.

Table 2 contains values of regression coefficients [Eq. (1)]. It also shows the results and grades from model adequacy F_a and significance of mathematical model coefficients. Values of the coefficients which can be neglected with probability of $\alpha = 0.05$ are marked with *.

In **Table 3**, are results of modeled cutting forces with genetic algorithms are shown. **Table 4** contains exponents which are generated by genetic algorithms according the Eq. (1). Process of generating the coefficients was carried out during 5000 generations with 50 individuals. From which 5 were elite individuals and rest were created by 0.6 crossover fractions and the rest of the generation was created by mutation.

Table 5 features the comparison of success rate of these two methods of coefficients determination. Average errors in deviation of calculated resp. modeled values from experimentally obtained values are shown. It can be seen that genetic algorithms generated more suitable coefficients and thus produced smaller error for most of the forces and materials except for tangential force F_r and for steel EN 34Cr4.

From **Table 5**, it can be concluded that both techniques can be used for cutting forces modeling but genetic algorithms having a slight advantage.

Influence of cutting conditions on grinding forces F_t and F_n for both workpiece material (EN 18CrNi8 and EN 34Cr4) is shown in **Figure 4** for workpiece speed, in **Figure 5** for the feed rate and for the depth of cut in **Figure 6**.

	EN 18CrNi8		EN 34Cr4	
	F_t	F_n	F_t	F_n
C	125.3	229.8	52.03	296.1
x	0.016*	0.232	0.104	0.270
y	0.073*	0.236	0.038*	0.273
z	0.590	0.850	0.654	0.945
F_a	3.069	0.740	1.775	5.389

Table 2. Coefficients in Eq. (1), calculated by response surface methodology.

No.	Machining factor			Experimentally measured values				Modeled values by genetic algorithms			
				EN 18CrNi8		EN 34Cr4		EN 18CrNi8		EN 34Cr4	
	v_t [m/min]	s_a [mm/rev]	a [mm]	F_t [N]	F_n [N]	F_t [N]	F_n [N]	F_t [N]	F_n [N]	F_t [N]	F_n [N]
1	18.4	20	0.01	11.8	17	10.9	17.8	10.64	17.35	10.19	17.60
2	36.8	20	0.01	12.4	17.8	11.8	19.8	11.28	18.81	11.65	19.79
3	18.4	30	0.01	12.3	18.4	13	18.9	12.31	22.08	11.54	21.37
4	36.8	30	0.01	12.9	19.8	13.2	21.1	13.06	23.94	13.19	24.03
5	18.4	20	0.02	16.1	29	17.4	29	14.41	24.51	14.49	24.60
6	36.8	20	0.02	16.6	31.5	17.9	31.2	15.28	26.57	16.57	27.67
7	18.4	30	0.02	17.2	31.2	18.8	33.1	16.68	31.20	16.40	29.87
8	36.8	30	0.02	17.5	33.3	20	33.6	17.69	33.82	18.75	33.60
9	26	25	0.014	12.1	25.4	12.3	24.8	13.76	24.39	13.84	24.43
10	26	25	0.014	12	25.3	13.5	24.7	13.76	24.39	13.84	24.43
11	26	25	0.014	12.6	24.5	12.2	24	13.76	24.39	13.84	24.43
12	26	25	0.014	12.8	24.3	14	24.1	13.76	24.39	13.84	24.43
13	16	25	0.014	13.6	23.1	12.6	22.8	13.2	23.05	12.60	22.50
14	42.4	25	0.014	14.2	25.6	13.6	25.6	14.34	25.82	15.21	26.54
15	26	18.4	0.014	14.4	22.1	12.4	23.1	12.31	20.32	12.60	21.09
16	26	32.6	0.014	15.5	28.2	14.1	24.3	15.14	28.57	15.01	27.74
17	26	25	0.0086	11	19.2	10.8	19	11.11	19.13	10.80	19.31
18	26	25	0.023	17.1	33.2	18.1	31.1	17.1	31.24	17.81	31.06
19	16	25	0.014	13.4	23	12.1	22.5	13.2	23.05	12.60	22.50
20	42.4	25	0.014	14.5	25.8	13.9	25.7	14.34	25.82	15.21	26.54
21	26	18.4	0.014	14.2	22.9	12.6	23.3	12.31	20.32	12.60	21.09
22	26	32.6	0.014	15	28.1	14.6	24.1	15.14	28.57	15.01	27.74
23	26	25	0.0086	11.1	19.2	11	19.6	11.11	19.13	10.80	19.31
24	26	25	0.023	17.6	33.3	18.5	31.8	17.1	31.24	17.81	31.06

Table 3. Measured and modeled values of cutting forces.

	EN 18CrNi8		EN 34Cr4	
	F_t	F_n	F_t	F_n
C	21.165	20.637	24.130	23.674
x	0.085	0.116	0.193	0.169
y	0.361	0.595	0.306	0.479
z	0.438	0.498	0.508	0.483

Table 4. Coefficients in Eq. (1), generated with genetic algorithms.

	Response surface methodology				Genetic algorithms			
	EN 18CrNi8		EN 34Cr4		EN 18CrNi8		EN 34Cr4	
	F_t	F_r	F_t	F_r	F_t	F_r	F_t	F_r
Average error %	5.96	6.63	7.98	5.14	5.39	5.25	5.63	5.48

Table 5. Comparison of the average errors made by response surface methodology and genetic algorithms.

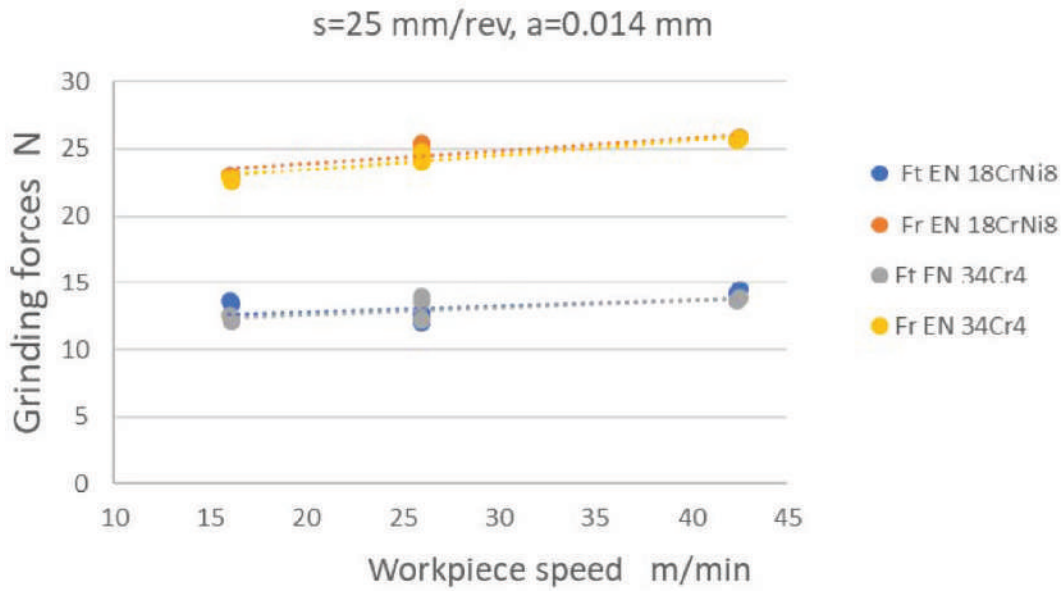


Figure 4. Influence of the workpiece speed on grinding forces.

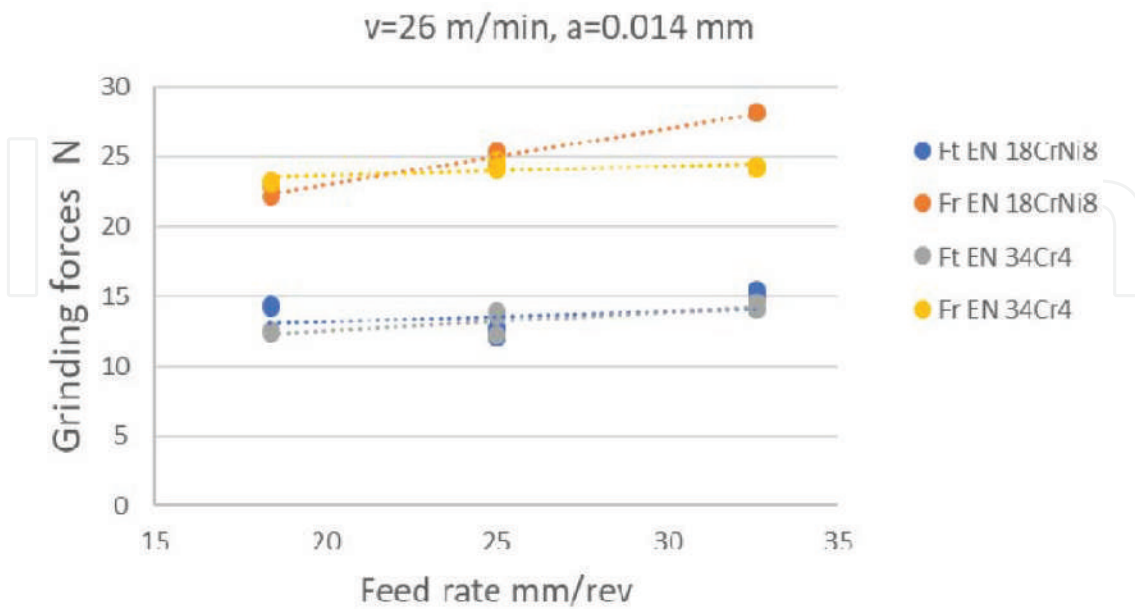


Figure 5. Influence of the feed rate on grinding forces.

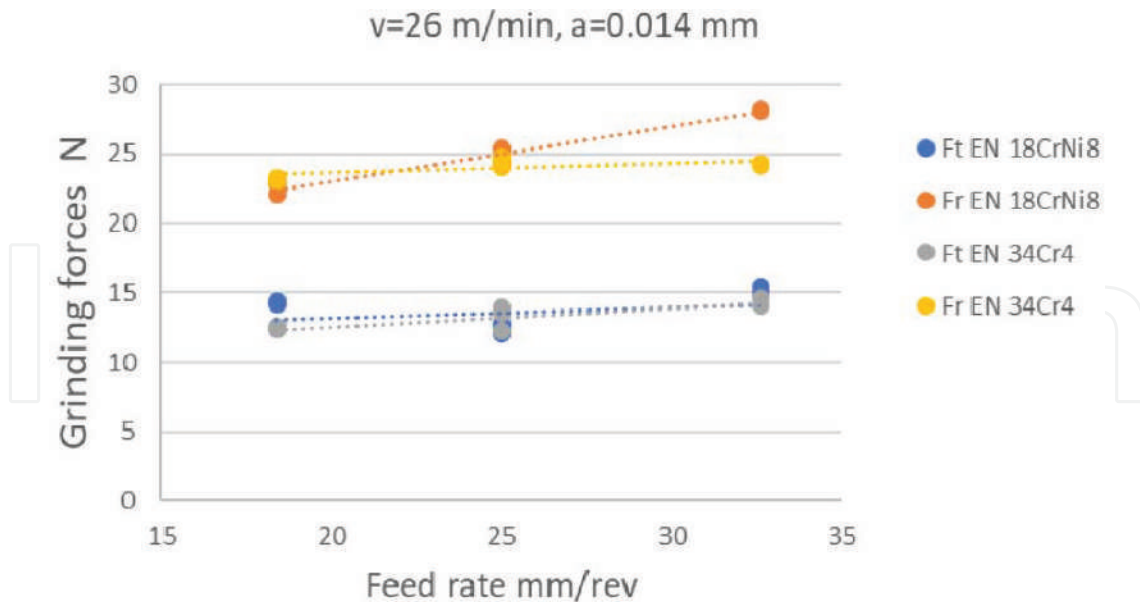


Figure 6. Influence of the depth of cut on grinding forces.

From **Figures 4–6**, it can be noticed that all input parameters, significantly influence increasing of cutting forces during cylindrical grinding process. Depth of cut has the highest influence on grinding forces followed by workpiece speed and then feed rate. This conclusion is valid for both study materials in study.

3.2. Creep-feed grinding

An example of measurement results of the cutting force during creep-feed grinding, two wheels with similar characteristics but different manufacturers, is shown in **Figure 7**. It can be concluded that for the same processing conditions obtained different values of force components sanding, or about the same dynamic character.

Figures 8 and 9 are given depending on the specific components of cutting forces, as well as their relationship F'_n/F'_v , depending on the cutting depth and the workpiece speed for both selected wheels. With diagrams shown it can be concluded that with increased cutting depth grinding forces are increasing and decrease with increasing the workpiece speed, because of cutting depth is decreasing.

Relationship of cutting force in grinding depends on the elements of the cutting regime, and a constant specific productivity of grinding, is shown in **Figure 10**. The diagram shows that compared to conventional grinding, in creep-feed grinding cutting forces appear higher for both grinding wheels.

The ratio of normal and tangential grinding forces moved to within 2–4, except that higher values related to creep-feed grinding for both grinding wheels versus the workpiece speed.

Input parameters significantly influence increase in specific cutting forces during creep-feed grinding process. Depth of cut has the highest influence on grinding forces have depth of cut,

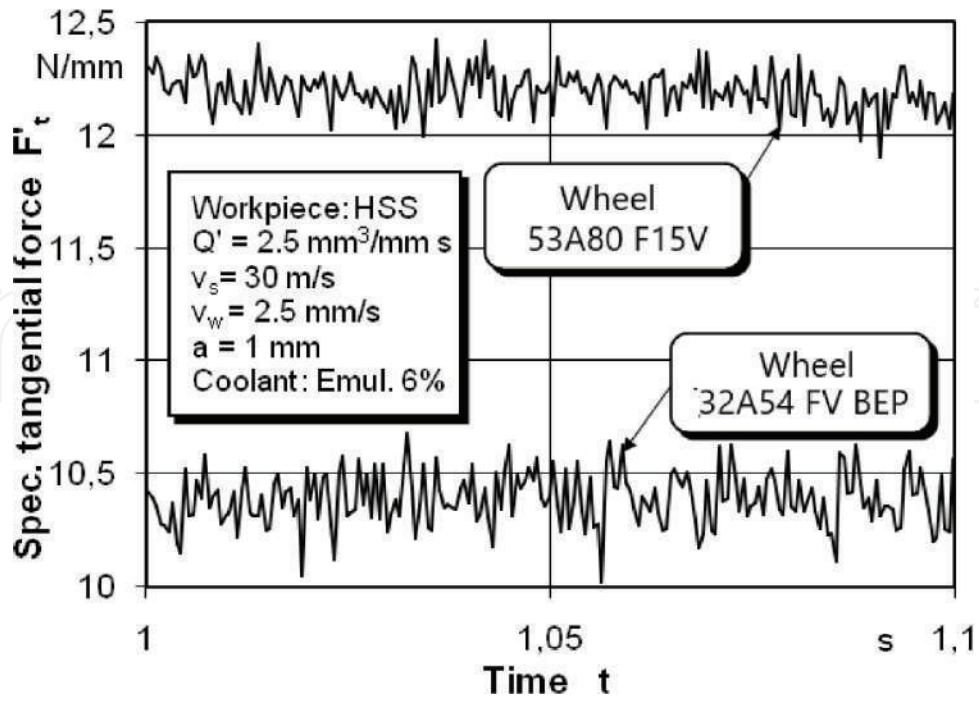


Figure 7. Value and character of the measured tangential grinding force components.

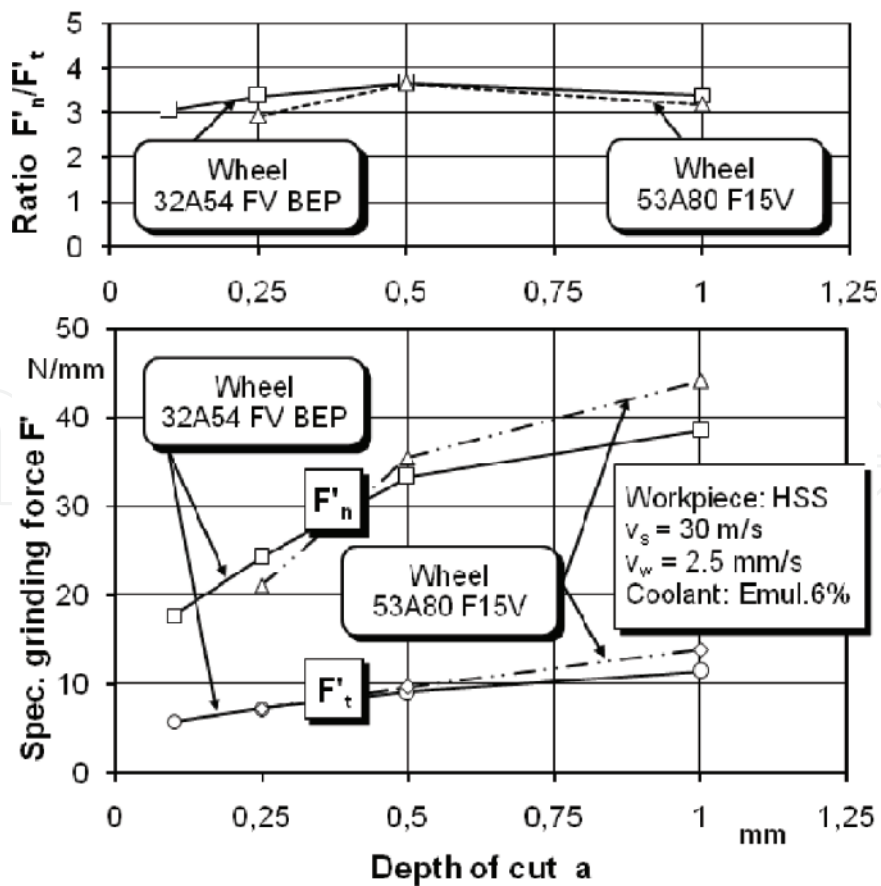


Figure 8. The grinding forces versus the depth of cut.

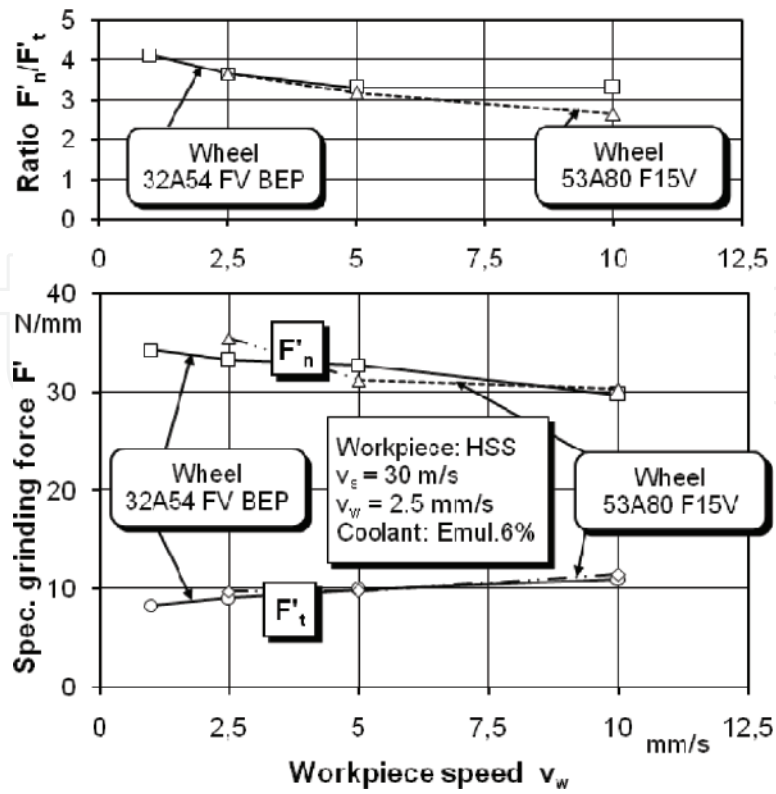


Figure 9. The grinding forces versus the workpiece speed.

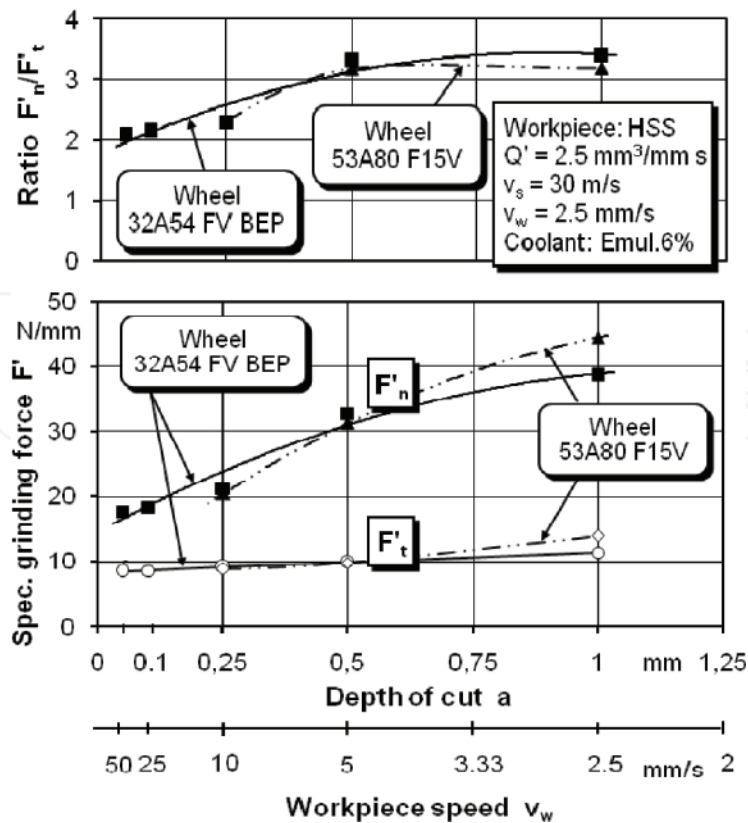


Figure 10. Specific grinding force versus the cutting regime for creep-feed grinding.

while workpiece speed has low influence on grinding forces. Increasing workpiece speed decreases specific grinding forces for both used grinding wheels.

4. Conclusions

Based on stated earlier, following can be concluded:

- Presented dynamometers can be successfully used for measurement of cutting forces during cylindrical grinding.
- Defined mathematical model of cutting forces F_t and F_r are adequate
- Influential elements of machining parameters on cutting forces are determined.
- Genetic algorithms are suitable for generating the coefficients for cutting force modeling.
- Creep-feed grinding reduces processing time, but also increases the cutting force
- Cutting forces primarily depend on the type of workpiece material and elements of its process
- Cutting forces during creep-feed grinding, due to a greater number of active abrasive grains into engagement with the workpiece material, are significantly higher compared to conventional grinding
- The grinding forces, the increasing length of contact of the grinding wheel and workpiece material, with increasing depth of cut;
- Increase the speed of the workpiece grinding forces decrease because it reduces the cross-section of the affected layers of material by grinding grain;
- Greater grinding force ratio can be observed in creep-feed;
- Cutting forces during creep-feed grinding allow identification of the energy balance of machine tools and estimation of the level of accuracy for different machining conditions

Acknowledgements

The Technological Development program Republic of Serbia, supported this TR 35015 project. For their support authors show great appreciation.

Nomenclature

v_r (m/min)	workpiece speed
s_a (mm/rev)	feed rate

a (mm)	depth of cut a (mm)
v_w (m/min)	workpiece speed creep-feed grinding
v_s (m/s)	grinding wheel speed
F_t (N)	tangential force
F_n (N)	normal force
F_a (N)	axial force
λ	grinding ratio
b	(mm) width of grinding
F_t', F_n' (N/mm)	specific grinding force:
u (n/mm ²)	specific grinding energy
h_m (mm)	grinding depth
Q' (mm ³ /mm·s)	specific material removal rate is
P' (W/mm)	specific grinding power

Author details

Pavel Kovač* and Marin Gostimirović

*Address all correspondence to: pkovac@uns.ac.rs

Faculty of Technical Sciences, University of Novi Sad, Novi Sad, Serbia

References

- [1] Rowe WB. Principles of Modern Grinding Technology. Boston: William Andrew Publishing; 2009
- [2] Chang HC, Wang JJ. A new model for grinding force prediction and analysis. International Journal of Machine Tools & Manufacture. 2008;48:1335-1344
- [3] Guo C, Campomanes M, Mcintosh D, Becze C, Green T, Malkin S. Optimization of continuous dress creep-feed form grinding process. CIRP Annals – Manufacturing Technology. 2003;52(1):259-262
- [4] Holešovski F, Hrala M, Stančik L. Measurement of cutting forces in the centre grinder. Manufacturing Technology Journal. 2005;5
- [5] Aslan D, Budak E. Semi-analytical force model for grinding operations. Procedia CIRP. 2014;14:7-12. DOI: 10.1016/j.procir.2014.03.073

- [6] Patnaik Durgumahanti US, Singh V, Venkateswara Ra P. A new model for grinding force prediction and analysis. *International Journal of Machine Tools and Manufacture*. 2010;**50**(3):231-240
- [7] Yao C, Wang T, Xiao W, Huang X, Ren J. Experimental study on grinding force and grinding temperature of Aermet 100 steel in surface grinding. *Journal of Materials Processing Technology*. 2014;**214**:2191-2199
- [8] Kopač J, Krajnik P. High-performance grinding – A review. *Journal of Materials Processing Technology*. 2006;**175**(1-3):278-284
- [9] Liu Q, Chen X, Wang Y, Gindy N. Empirical modelling of grinding force based on multivariate analysis. *Journal of Materials Processing Technology*. 2008;**203**:420-430
- [10] Gostimirovic M, Sekulic M, Kopač J, Kovac P. Optimal control of workpiece thermal state in creep-feed grinding using inverse heat conduction analysis. *Strojniški vestnik – Journal of Mechanical Engineering*. 2011;**57**(10):730-738
- [11] Gostimirovic M, Kovac P, Jesic D, Skoric B, Savkovic B. Surface layer properties of the workpiece material in high performance grinding. *Meta*. 2012;**51**(1):105-108
- [12] Gostimirovic M, Kovac P, Sekulic M. An inverse heat transfer problem for optimization of the thermal process in machining. *Sadhana*. 2011;**36**(4):489-504
- [13] Kovač P. Modeling of Machining Process- Factorial Experimental Plans (in Serbian). Novi Sad: FTS; 2006
- [14] Pucovski V, Kovač P, Tolnay M, Savković B, Rodić D. The adequate type of function for modeling tool life selection by the use of genetic algorithms. *Journal of Production Engineering*. 2012;**15**(1):25-28
- [15] Mishra VK, Salonitis K. Empirical estimation of grinding specific forces and energy based on a modified Werner grinding model. *Procedia CIRP*. 2013;**8**:287-292